Journal of Volcanology and Geothermal Research 282 (2014) 60–76

Contents lists available at ScienceDirect

Journal of Volcanology and Geothermal Research

journal homepage: www.elsevier.com/locate/jvolgeores

Physico-chemical and environmental controls on siliceous sinter formation at the high-altitude El Tatio geothermal field, Chile

Constanza Nicolau [a,b,*], Martin Reich [a,b], Bridget Lynne [c]

[a] Department of Geology, Universidad de Chile, Plaza Ercilla 803, Santiago, Chile
[b] Andean Geothermal Center of Excellence, Universidad de Chile, Plaza Ercilla 803, Santiago, Chile
[c] Department of Engineering Science, University of Auckland, 70 Symonds Street, Auckland, New Zealand

ARTICLE INFO

Article history:
Received 7 February 2014
Accepted 10 June 2014
Available online 24 June 2014

Keywords:
El Tatio
Siliceous sinter
Sinter mineralogy
Hot spring rocks

ABSTRACT

El Tatio geothermal field is located 4270 m above sea level in the Altiplano, northern Chile. Siliceous sinter deposits from El Tatio were studied to understand the influence of water chemistry and the extreme climatic conditions on their textures and mineralogy. The results of this study show that the mineralogy of El Tatio sinters include of opal-A and accessory minerals, such as halite, gypsum and cahnite ($Ca_4B_2As_2O_{12}{\cdot}4H_2O$), which precipitate by full evaporation of high arsenic, boron and calcium thermal waters. El Tatio sinters show a high degree of structural disorder, probably linked to cation incorporation into the silica structure and/or the occurrence of micro- to nano-scale accessory minerals. The high content of cations in the thermal waters is strongly tied to relatively high silica precipitation rates considering silica concentration in water (147–285 mg/l SiO_2). Precipitation rate reach 2.5 kg/m^2 per year based on *in situ* precipitation experiments. The particular environmental conditions of this high-altitude geothermal area that produce high water cooling rate and high evaporation rate, may also be responsible for the fast silica precipitation. Low environmental temperatures create freezing-related sinter textures (i.e., silica platelets and micro columns/ridges). Silicified microbial filaments are also characteristic of El Tatio sinters, and they are indicative of water temperature and hydrodynamic conditions at the moment of sinter formation. However, sinter textural interpretation in a high-altitude Andean context must be done carefully as specific relationships between microbial and hydrodynamic textures are found.

1. Introduction

Siliceous sinter deposits are hot spring related rocks formed by evaporation and cooling of near-neutral alkali-chloride thermal waters (Fournier and Rowe, 1966). Sinters are mainly composed of silica, although other minerals, such as halite, sylvite, realgar and native sulfur, can be present in minor amounts (Hampton et al., 2004; Handley et al., 2005; García-Valles et al., 2008; Tobler et al., 2008). The silica phases that compose siliceous sinters may include opal-A, opal-A/CT, opal-CT, opal-C, chalcedony, moganite and quartz, although the initial silica phase is always opal-A (Herdianita et al., 2000; Campbell et al., 2001; Lynne and Campbell, 2003, 2004; Rodgers et al., 2004; Lynne et al., 2005, 2008). Diagenetic transformations from opal-A to quartz occur via dehydration. The input of post-depositional heat and minor fluid are required to facilitate such transitions. Sinter diagenesis is not time-dependent and is greatly influenced by post-depositional events such as acidic steam condensate overprinting, secondary fluid circulation and burial (e.g., Lynne and Campbell, 2004; Lynne et al., 2005, 2008). Reported literature states that unaltered newly-deposited opal-A sinters have a low degree of structural order, evidenced by high Full Width at Half Maximum (FWHM) values (~8 °2) measured on X-Ray Diffraction traces, whereas more mature silica phases reveal lower values (down to 0.1 °2 for quartz; Lynne and Campbell, 2004; Lynne et al., 2005).

Sinter deposits are important in geothermal and ore exploration due to their direct link to high temperature (>175 °C) hydrothermal reservoirs at depth (Fournier and Rowe, 1966). They are also of interest because they record the environmental and hydrological conditions at the time of sinter formation along with the attributes of the biological population that thrives in the thermal water (Walter, 1976; Cady and Farmer, 1996; Hinman and Lindstrom, 1996; Konhauser and Ferris, 1996; Jones et al., 1997a; Campbell et al., 2001; Konhauser et al., 2001; Lowe et al., 2001; Jones et al., 2003; Guidry and Chafetz, 2003; Lynne and Campbell, 2003; Handley et al., 2005; Schinteie et al., 2007). Additionally, the study of sinter formation at hot spring settings provides insights to early Earth environments and can contribute to our understanding of the development of life in extreme environments (e.g. Farmer, 1998; Farmer and Des Marais, 1999; Farmer, 2000; Westall et al., 2001; Konhauser et al., 2003).

Geothermal systems in northern Chile are commonly located along the Andes, at high altitude (>4000 m above the mean sea level). However, the mineralogical and chemical features of siliceous sinter deposits formed under this particular environment remain understudied. Previous

* Corresponding author at: Department of Geology, Universidad Mayor, Manuel Montt #367, Santiago, Chile. Tel.: +56 9 64078300.
E-mail address: cnicolau@ing.uchile.cl (C. Nicolau).

http://dx.doi.org/10.1016/j.jvolgeores.2014.06.012
0377-0273/

works at the El Tatio geyser field have focused on the aqueous and gas geochemistry of the thermal features (e.g., Cusicanqui et al., 1975; Giggenbach, 1978; Cortecci et al., 2005; Tassi et al., 2005, 2010), and a few studies have reported mineralogical characterizations of the sinters (Jones and Renaut, 1997; Glennon and Pfaff, 2003; Fernández-Turiel et al., 2005; García-Valles et al., 2008). Despite these studies, little is known about the physico-chemical factors that control silica precipitation and accumulation in high-altitude systems. This information is of utmost importance as the environmental conditions typical of high-altitude systems in the Andes such as, increased evaporation rates, lower surface boiling temperature, and large daily temperature oscillations, may have an important impact on silica precipitation kinetics.

In this work, we report new textural and mineralogical data of the high-altitude siliceous sinter deposits from the El Tatio geothermal field. By coupling these data to the hot-spring chemistry and the results from an *in situ* silica precipitation experiment carried out at the site, we show that siliceous sinter formation and their resulting textures depend not only on fluid geochemical controls but also on the environmental features that are typical of high-altitude environments.

2. Geological background

The El Tatio geothermal field (22°20′S and 68°W) is located in the Altiplano of northern Chile (Fig. 1), along the Salado river valley and its affluents. The geologic sequence that outcrops in the El Tatio area includes Jurassic marine sediments, Jurassic–Cretaceous meta-andesites and Cretaceous sediments; Miocene ignimbrites, andesites and volcanic agglomerates; and Plio–Holocene dacitic and rhyolitic ignimbrites, lavas and domes (Lahsen and Trujillo, 1976). Glacial, alluvial and colluvial deposits overlay this geologic sequence and are locally covered by siliceous sinter deposits (Lahsen and Trujillo, 1976; Fernández-Turiel et al., 2005). The hydrogeological model for El Tatio geothermal system, proposed by Cusicanqui et al. (1975) and Giggenbach (1978), involves a geothermal reservoir trapped in permeable rocks of Puripicar ignimbrite (Pliocene) and Rio Salado ignimbrite (Upper Miocene) and a second aquifer hosted in a dacitic unit (Pleistocene), sealed by silica deposits and clays.

At 4270 m above sea level, the El Tatio field is exposed to severe climatic conditions. The climate in this area is characterized by low precipitation rates (<100 mm/year). Rainfall is very seasonal, because this area is under the influence of the South American Summer Monsoon, with rains occurring from November to March (Zhou and Lau, 1998) that are particularly intense from December to March (Fernández-Turiel et al., 2005). The mean annual temperature ranges from 8 to 11 °C and the daily temperature variation often reaches 35 °C. In winter the temperature can fall down to −30 °C (Fernández-Turiel et al., 2005). The mean annual evaporation rate at El Tatio is 131.9 mm, reaching its maximum during December (183.2 mm) and minimum during June (72.8 mm) (DGA, 2010).

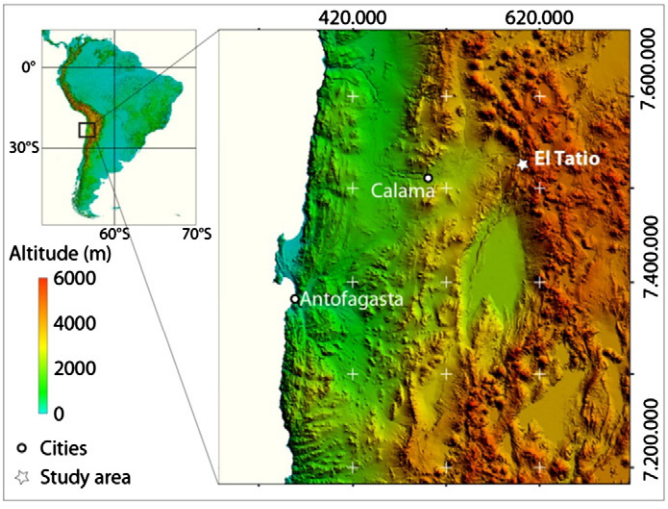

Fig. 1. Digital Elevation Model of the study site location in a regional context; coordinates are presented in the Universal Transverse Mercator system. Corner inset represents the study site location in South America; coordinates for the insert are presented in the Sexagesimal system.

Numerous surficial thermal features occur at the El Tatio field, covering an area of more than 10 km^2. These thermal features include fumaroles, geysers, hot springs, hot pools, boiling pools, mud pools, sinter deposits and hydrothermally-altered rocks. Previous studies have addressed the genesis of siliceous oncoids around geyser vents and hot pools, and the mineralogical variability of sinters related to diagenesis (Jones and Renaut, 1997; Fernández-Turiel et al., 2005; García-Valles et al., 2008). According to these studies, siliceous sinter deposits at El Tatio are mainly composed of non-crystalline silica phase, opal-A, with a minor occurrence of para-crystalline phases (opal-A/CT and opal-CT; Fernández-Turiel et al., 2005; García-Valles et al., 2008). Their chemical composition shows variable concentrations of Cl, Na, Ca, S, As, Sb and B (5–20 wt%; Fernández-Turiel et al., 2005; Landrum et al., 2009). Mineralogical studies reveal the common occurrence of accessory minerals such as halite [NaCl], sylvite [KCl] and realgar [AsS], and the rare occurrence of nobleite [$CaB_6O_{10} \cdot 4H_2O$], teruggite [$Ca_4MgAs_2B_{12}O_{22}(OH)_{12} \cdot 12(H_2O)$] and sassolite [$H_3BO_3$] (Rodgers et al., 2002a; García-Valles et al., 2008). In addition, a variety of biological communities of green bacteria, cyanobacteria, and diatoms thrive in the hot springs that form sinter deposits; their existence is largely dependent on the physico-chemical features of the thermal waters (Fernández-Turiel et al., 2005). Thermal water discharges at El Tatio have near neutral pH, are alkali-chloride in composition and display high concentrations of dissolved silica (SiO_2 < 3.6 mM), arsenic (As < 0.6 mM), boron (B < 17 mM) and antimony (Sb < 0.034 mM; Landrum et al., 2009).

3. Sinter textures background

Micro-textures and the diameter of silicified microbes in sinter deposits are used to reconstruct discharging fluid temperatures and environmental conditions at the moment of sinter formation (Cady and Farmer, 1996; Lowe et al., 2001; Guidry and Chafetz, 2003). In particular, filament diameters >5 μm typically indicate low-temperature (<35 °C) environments (Cady and Farmer, 1996; Walter et al., 1996; Jones et al., 1997b; Walter et al., 1998; Campbell et al., 2001; Lynne and Campbell, 2003; Lynne, 2012). Intermediate-diameter microbial filaments (<4 μm) usually thrive in warmer waters between ~35 and 60 °C (Hinman and Lindstrom, 1996; Farmer, 2000; Campbell et al., 2001). High-temperature settings host filamentous microbes of <1 μm diameter (Pierson and Castenholz, 1974).

According to Handley and Campbell (2011), different sinter textures can originate depending on the state of polymerization of silica at the moment of its deposition. Deposition of soluble monomeric or polymeric silica produces "vitreous" sinter fabric, and is common in acidic fluids or near-vent settings, whereas the deposition of colloids leads to the formation of porous granular sinter. Mixed solutions produce dense cemented granular sinter due to the precipitation of soluble silica at colloid joints (Iler, 1979; Rodgers et al., 2002b). In high-temperature (>60 °C) settings, various sinter textures can be produced, including digitate sinter and columnar sinter (e.g. Lynne, 2012). The former is produced by silica precipitation over pool rims during overflowing events at intermittently overflowing pools and channels (Lowe and Braunstein, 2003; Lynne, 2012), whereas the latter originates by rapid cooling and evaporation of the ejected water droplets in near-vent settings (Braunstein and Lowe, 2001; Jones and Renaut, 2003; Lowe and Braunstein, 2003; Lynne, 2012)

4. Methods

Five sampling sites were selected at El Tatio based on (i) different hydrodynamic characteristics, including eruptive and quiescent pools, and their respective discharge channels, and (ii) different macroscopic textures and coloration of their associated siliceous sinter deposit. The sampling sites were described in terms of the physico-chemical and hydrodynamic characteristics. Water temperature and pH were measured at each site, and water and sinter samples were collected. The sampling sites are located along a north-east trending valley, where most of the sinter deposits are situated (Fig. 2A). Additionally, an *in situ* experiment was developed at one sampling site (site 3; Fig. 2B) to determine the silica precipitation rate at El Tatio.

4.1. Chemical analysis of water samples

At each site, thermal water was filtered using a 0.45 μm millipore membrane and then collected in 200 ml bottles. Samples for cation/metal analysis were acidified with 2 ml of HNO_3 after filtering. Water samples were analyzed at the Department of Geology, University of Chile for major and minor cations (Si, Ca^{2+}, K^{+}, Mg^{2+}, Na^{+}, B^{3+}, Fe^{2+}, Li^{+}, Mn^{2+}, Al^{3+}, As^{3+} and Sr^{2+}) and anions (Cl^{-}, Br^{-}, NO_3^{-}, SO_4^{2-}) using inductively coupled plasma optical emission spectrometry (ICP-OES: Perkin Elmer Optima 7300 V) and ion chromatography (IC: Metrohm 861), respectively. Carbonate species concentrations were measured by acidimetric titration with back titration, following the Giggenbach and Gouguel (1989) methods.

4.2. Mineralogical and textural determinations of sinter samples

X-Ray Diffraction (XRD) of the sinter samples were carried out to determine the silica phase. Dry sinter samples were ground in a mortar and scanned at 0.6°2 /min, with a step size of 0.01°, from 10 to 40°2 , in a Phillips PW1130/00 Diffractometer, at the University of Auckland, New Zealand. Operating conditions were 40 kV and 20 mA, using CuKα radiation (λα = 1.54051 Å). Following the methods in Lynne (2007), XRD traces were not digitally manipulated; for each sample the Full Width at Half Maximum (FWHM) was measured fitting the

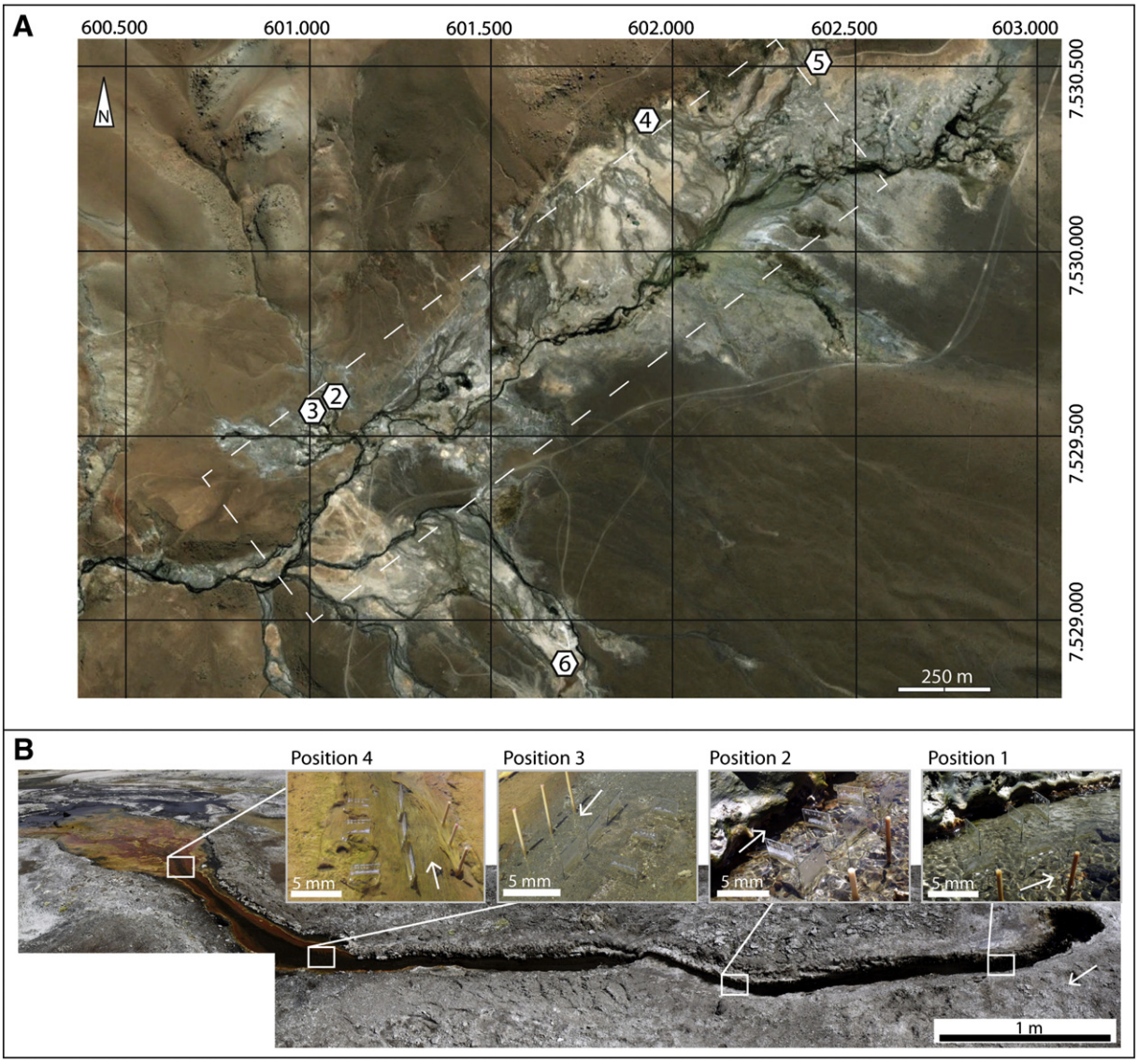

Fig. 2. Sampling sites. A: Sampling sites location along the northern river valley at El Tatio geothermal field. Dashed line rectangle indicates the main area with sinter outcrops, which is used for age calculations. B: Setting of the silica accumulation rate experiment at El Tatio, Chile. The white rectangles show the location of the glass slides sets along the discharge channel. Upper pictures illustrate the orientation of the glass slides with respect to the water flow (white arrows).

curve and base line manually. FWHM measurements were used to compare the degree of lattice disorder between different non-crystalline phases. To detect the presence of other mineral phases, the same samples were scanned at 3.6 °2 /min, with a step size of 0.02°, and from 2 to 80 °2 . This additional XRD analysis was carried out in a Siemens D-5000 Diffractometer at the Physics Department of the Universidad de Chile, Chile, and the conditions were 40 kV and 30 mA. The identification of mineral phases was carried out using the MacDiff4.2.6 software and MSA Crystal Structure Database (Downs and Hall-Wallace, 2003).

In order to obtain morphological, textural and semi-quantitative chemical data, sinter samples were analyzed using scanning electron microscope (SEM) techniques. Millimeter- to centimeter-scale samples were mounted on aluminum stubs and coated with a layer of either platinum or gold. Samples were examined using a FEI Quanta 200 F field-emission-gun SEM, at the Earth and Materials Science Department, University of Auckland, New Zealand, and a FEI Quanta 200 MK2 SEM, at the Universidad de Chile, Chile. Operating conditions were 5 to 20 keV accelerating voltage, spot size of 1 to 4, and a working distance of 10 to 18 mm. Secondary electron (SE) detection was used to obtain topographic images of the fresh surface of the sinter sample and to recognize the morphology of silica and other mineral phases, and their textural relationships. Energy-dispersive X-ray spectrometry (EDS) was used to determine the major elements of individual mineral phases. EDS operating conditions were 20 keV, a spot size of 5 and a working distance of 10 to 18 mm. Additionally, thin sections were examined under a polarizing microscope to identify micro-to-millimeter scale sinter textures and determine the presence of microbes, minerals and/or lithic components within silica laminations.

4.3. Silica precipitation rate determination

An *in situ* experiment was developed at El Tatio to measure the silica precipitation rate by placing glass slides along the discharge channel of a selected hot spring that correspond to site 3. The slides were collected after 1, 2, 9 and 10 months, and then the amount of silica precipitated over the slides was measured to obtain an experimental silica precipitation rate. Glass slides were situated along a discharge channel of a bubbling hot pool with a temperature of 82 °C, a pH of 6.5 and a measured dissolved silica concentration of 147 mg/l. Glass slides were weighed prior to placement in the hot spring channel. Slides were situated along the discharge channel, at four locations, about 3 meters apart. At each site a set of six glass slides were placed. Half of the slides were positioned perpendicular to the water flow direction, while the other half parallel (Fig. 2B). The set-up phase of the experiment took place during January 2012. Three sample collection stages were followed: March, October and November 2012, and during each visit glass slides were collected and placed into sterilized 500 ml plastic tubes. Additionally, one glass slide perpendicular to the water flow was added to each spot in March 2012, and removed a year later in April 2013. Samples were labeled according to the month of placement of the slides and the month of collection. Samples were dried at room temperature. The mass of silica precipitate was estimated by subtracting the original weight of the glass slide from the total weight of the samples once dried.

Environmental conditions (ambient temperature, humidity, wind velocity and direction) were measured *in situ* at the beginning of the experiment using a thermo-anemometer and a portable hygrometer. An experimental evaporation rate was estimated *in situ* by measuring the wetted area and the time it took to dry a known amount of water (1 ml or 0.5 ml) poured onto a dry sinter surface.

5. Results

5.1. Geochemistry of thermal water samples

The studied sites (Fig. 2) consisted of sodium-chloride hot pools, boiling pools and quiescent pools that are associated with extensive siliceous sinter deposits. Chemical data of the studied hot-springs is presented in Table 1. The pH of water in the pools is near neutral and ranges from 6.5 to 7.5, while the water temperature ranges from 76.9 to 87.6 °C. The latter correspond to boiling temperature at 4200 m above sea level. Thermal water chemistry is characterized by a high concentration of dissolved SiO_2 (147–285 mg/l), Ca (156–306 mg/l) and K (192–848 mg/l). The As content is high in all samples (>17 mg/l), but the highest values occur at sites 4 and 5 (31 mg/l). The S content is higher at site 3 (378 mg/l), intermediate at site 2 (105 mg/l) and site 6 (146 mg/l), and low at sites 4 and 5 (<90 mg/l). Water samples are undersaturated with respect to silica at the sampling temperature (Fig. 3). Only at site 4, the silica concentration is close to saturation (silica saturation concentration at site 4 is 291.67 mg/l)

No significant variation in the concentrations of most cations and anions was detected during the 11-month period (January to November). However, the SO_4^{2-} content of water was remarkably higher in April

Table 1
El Tatio thermal springs geochemical data.

Sample ID	Site 2	Site 3[1]	Site 3[2]	Site 3[3]	Site 4	Site 5	Site 6
T	86.2	82.3	82.3	83	82.7	76.9	87.6
pH	7.4	6.5	6.37	6.39	7.3	7.1	7.4
Ca	157	158	147	142	268	292	307
K	239	236	219	220	849	534	192
Mg	6.4	5.8	5.7	5.3	0.3	0.6	2.0
Na	2230	2200	2143	2151	4678	4212	3555
Al	0.0	0.0	0.0	1.4	0.0	0.0	0.1
B	40	41	112	109	84	82	71
Fe	0.11	0.16	0.83	0.23	0.01	0.01	0.01
Li	24	24	22	22	61	59	42
Mn	0.5	0.4	0.6	0.5	0.2	0.1	0.1
Sr	2.3	2.3	2.5	2.4	4.3	4.6	4.4
SiO_2	147	147	140	133	285	223	223
As	18	18	16	17	31	32	25
Cl	4211	3480	4103	4513	9119	8819	6995
Br	16.6	154.5	8.7	9.3	91.2	93.4	89.3
NO_3	160.1	31.7	4.4	6.4	100.7	104.9	113.2
SO_4	105	378	36	37	89	81	146
HCO_3	117	131	124	127	4.3	0.0	32
SiO_2 sat. [4]	305.44	290.12	290.12	292.84	291.67	269.67	311.04
SiO_2 sat. ratio[5]	0.48	0.51	0.48	0.45	0.98	0.83	0.72

Temperatures are in °C. Concentrations are expressed in mg/l. [1] january 2012; [2] march 2012; [3] april 2013. [4] SiO_2 sat. corresponds to silica saturation concentration at the sampling temperature as calculated by the equation: $\log C = -731/T + 4.52$; where C is the silica concentration in mg/l and T is the temperature in Kelvin (Fournier and Rowe, 1966). [5] SiO_2 sat. ratio corresponds SiO_2 content of water samples divided by the saturation concentration at the sampling temperature.

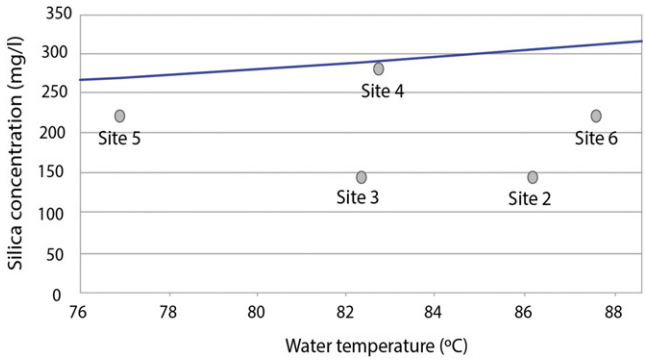

Fig. 3. Silica concentration versus water temperature plot. The blue line correspond to the silica saturation curve.

(~380 mg/l) than in November and October (~35 mg/l), and conversely, the Cl^- content was lower in April (~3500 mg/l) than in October and November (>4000 mg/l).

The selected sites can be separated in two compositional groups: sites 2 and 3 show the lowest concentration of chlorine (<5000 mg/l), sodium (<3000 mg/l) and lithium (~24 mg/l), and the highest concentration of bicarbonate (>100 mg/l) and magnesium (~6 mg/l), which is related to a mixture of thermal and meteoric water. Conversely, sites 4 and 5 show the higher concentration of chlorine (>6000 mg/l), sodium (>3500 mg/l) and lithium (~60 mg/l), and the lower concentration of bicarbonate (<5 mg/l), and magnesium (<2 mg/l), which reflects less influence of meteoric water.

5.2. Sinter mineralogy and textures

For this study the El Tatio sinters are described in two separated groups based on their color (white vs. colored sinters). Tables 2–4 summarize the characteristics of the analyzed sinter samples, including silica phase morphology and diameter, occurrence of mineral phases and lithic fragments in the sinter deposits, as well as the biological features of the samples. Sites 2 and 6 are eruptive pools, site 4 is an eruptive cyclic boiling pool, site 3 is quiescent and bubbling with a few eruptive events, and site 5 is a non-bubbling, non-boiling pool. White sinter deposits were identified at sites 2 and 4, which correspond to eruptive pools, and also at site 5, which correspond to a quiescent pool. Colored sinters were found at sites 3 and 6, which correspond to pools that show eruptive behavior. However, eruptive events at site 3 are less frequent and vigorous than at site 6.

White sinter deposits (samples M2.1, M2.3, M4.1, M4.2 and M5) show a variety of macro-textures including columnar textures (Fig. 4 A, B, C), and digitate rims and islands (Fig. 4 D). The internal structure is usually porous and laminated (Fig. 4 E), although some samples show vitreous massive internal laminations. The macroscopic laminations observed at the macro-scale were also observed in thin sections, and sinter laminations appear light to dark brown under the petrographic microscope (Fig. 4 F). White sinters are mainly composed of opal-A, and show scarce occurrence of other mineral phases such as halite as observed by SEM and shown by XRD traces (Fig. 5 A). The FWHM parameter for these samples range from 7.8 to 9.4 °2 (Table 3). The opal-A morphology correspond to smooth spheres that can be randomly aggregated forming botryoidal clusters (Fig. 5 B) or evenly coalesced forming well defined layers (Fig. 5 C). The micro-textures observed under the SEM include silica platelets commonly found on the sinter surface (Fig. 5 D), porous and massive silica laminations (Fig. 5 E), and micro-columns and ridges (Fig. 5 F). Filamentous microbes of various diameter (0.8 to 5 μm diameter), pollen spores and plant material were entombed within the sinter deposit.

Colored sinter samples were collected from a bubbling pool and a boiling pool which correspond to sites 3 and 6 (M3, M3.2 and M6.4). The sinter samples from the near-vent settings shows splashing and overflowing textures at the pool rim, and columnar textures in the sinter island at the beginning of the discharge channel at site 3 (Fig. 6 A, B). The sinter deposit is composed by macroscopic laminations that show a large variability in color, including white, light brown, grey, yellow and dark red (Fig. 6 C). A red crust is present at the surface of the deposit in sub-aerial zones, while a black crust is present at sub-aqueous zones (Fig. 6 C, D). In cross-section, the deposit shows horizontal sinuous laminations resembling incipient micro-columns (Fig. 6 E). Under the petrographic microscope, the light-to-dark brown laminations alternate with reddish laminations (Fig. 6 F).

The XRD data of the colored sinter samples show broadbands that correspond to opal-A, but also show abundant accessory mineral peaks (Fig. 7 A). The FWHM value for these samples range from 8.0 to

Table 2
Silica phase morphology and diameter (μm) in El Tatio sinters.

Sinter nature	Sample ID	Smooth micro- and nano-spheres	Bumpy micro-spheres	Rough micro-spheres	Spiky micro-spheres
white sinter	M2.1	0.2–2.2			
	M2.3	0.3–2.2			
	M4.1	0.3–2.5	2.3–4		
	M4.2	0.5–1.5	2–5		
	M5	0.2–3	0.4–1.5		
colored sinter	M3B	0.3–2.3	1–3	2–3	
	M3.2	0.2–2	2–3.5		
	M6.4	0.5–2	2.5–5	0.5–3.5	3–7

Table 3
XRD characteristics of silica phase and mineral and lithic components of El Tatio sinters.

Sinter nature	SampleID	FWHM (°2θ)	Apex position (°2θ)	Max. intensity (counts/sec)	Mineral phases					Lithic Fragments
white sinter	M2.1	9.4	22.9	276	G					
	M2.3	8.3	22.5	230		H				yes
	M4.2	7.8	22.4	321	G	H				
	M5	7.9	22.2	287	G	H				
colored sinter	M3	12.5	23.7	174	G	H	F	C		
	M3.2	8.2	22.8	203		H	F			yes
	M6.4	8.0	22.8	327			F	C	N	

Capital letters indicate the presence of mineral phases: G = gypsum, H = halite, F = flower-like crystals, C = cahnite, N = needle-like crystals

Table 4
Biotic components of El Tatio sinter samples.

SampleID	Biological material				MF diameter (μm)
M2.1					
M2.3				MF	2.5
M4.2		Pl	Po		
M5				MF	1–1.5
M3				MF	0.8–3
M3.2		Pl	Po	MF	0.7–1.5; 10
M6.4	D	Pl		MF	3

D = diatoms, Pl = plant material, Po = pollen spores, MF = microbial filaments.

12.5 °2 . At the micro-scale, colored sinters are composed of individual and aggregated opal-A spheres (Fig. 7 B, C), similar to those observed in the white sinters. However, SEM observations reveal that the morphology of opal-A spheres from colored sinters include bumpy micro-spheres (Fig. 7 C), rough micro-spheres (Fig. 7 D), and spiky micro-spheres (Fig. 7 E). Opal-A spheres are commonly found forming massive laminations of variable thickness (Fig. 7 F). Rough micro-spheres are found in the laminations of colored sinters from sites 3 and 6, while spiky micro-spheres are only found in the sub-aquatic black crust of the samples from site 6. SEM-EDS chemical analysis of these spiky spheres reveals a high content of As (up to 18.4 %wt) and Fe (up to 15.3 %wt) and minor contents of other elements such as Ca (7.5 %wt) and Al (3.2 %wt). In colored sinter samples, microbial filaments, plant material and diatoms were also identified.

After the abundant and ubiquitous opal-A phase, SEM observations reveal that halite and gypsum are common minerals in El Tatio sinters, usually occurring at the surface of the deposits in both colored and white samples (Fig. 8 A, B). The XRD traces of the analyzed samples show the presence of halite (with peaks corresponding to 2.82 and 1.99 d-spacing), but also the occurrence of other mineral phases such as micas (with peaks corresponding to 9.94, 3.54, 2.81 and 2.62 d-spacings that agree with those of phlogopite), amphiboles (possibly hornblende with peaks corresponding to 8.1, 3.1, 2.82 and 1.99 d-

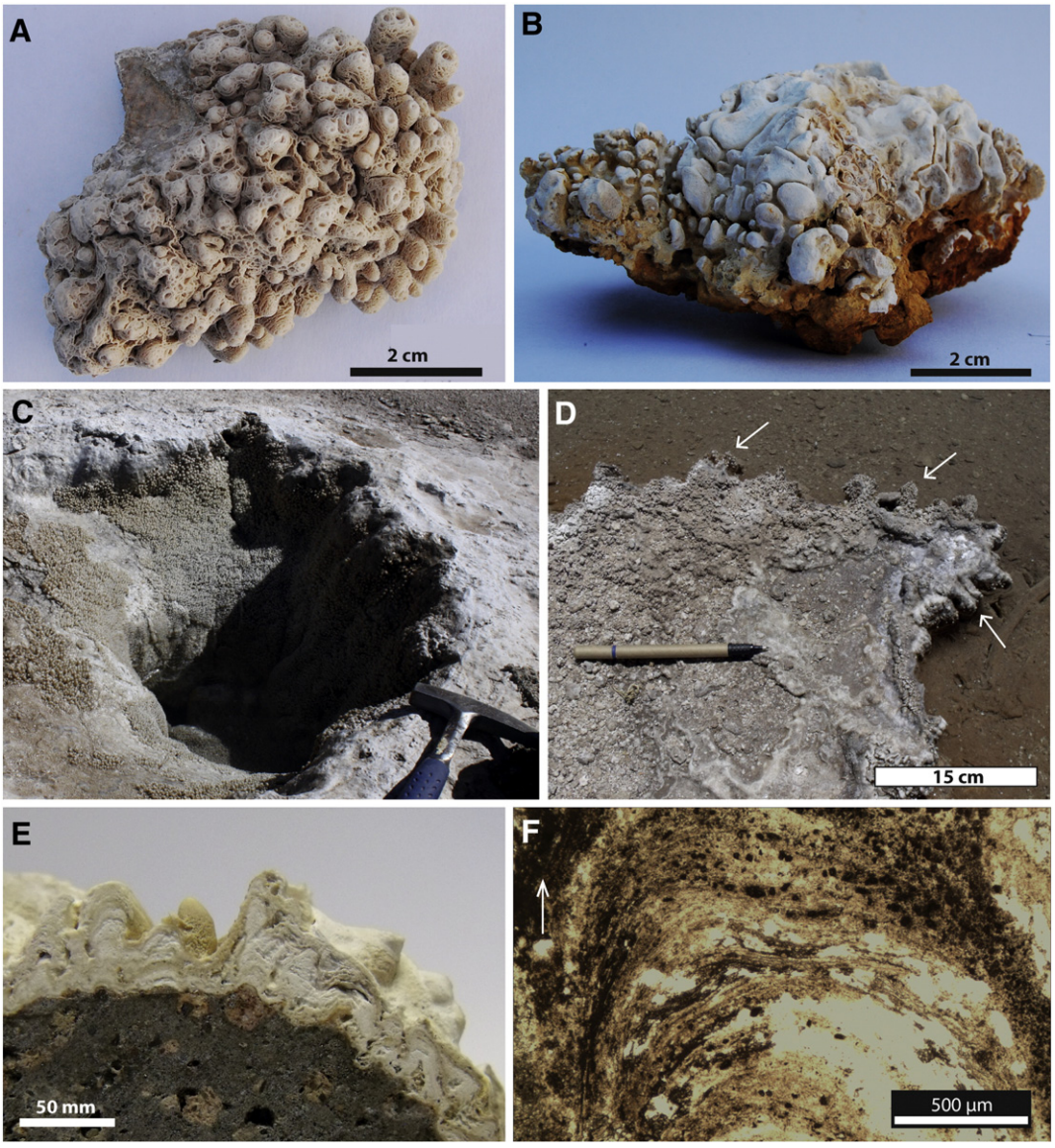

Fig. 4. White sinters: macroscopic characteristics and sampling sites. A: Columnar white sinter showing pits and crevices at the surface. B: Sinter deposit of site 4 forming around a cyclic eruptive pool (~82 °C water), it shows columnar texture on the pool rim, walls and bottom. C: Site 4 eruptive cyclic boiling pool and white sinter deposit that show mainly columnar texture. D: Sinter pool rim with digitate texture around a quiescent hot pool (~77 °C), site 5. E: Internal structure of a sinter sample from site 2. White lamminations are forming columns following the topography of the substrate. F: Photoghraph of the sample from E under the petrographic microscope. It shows white and brown laminations.

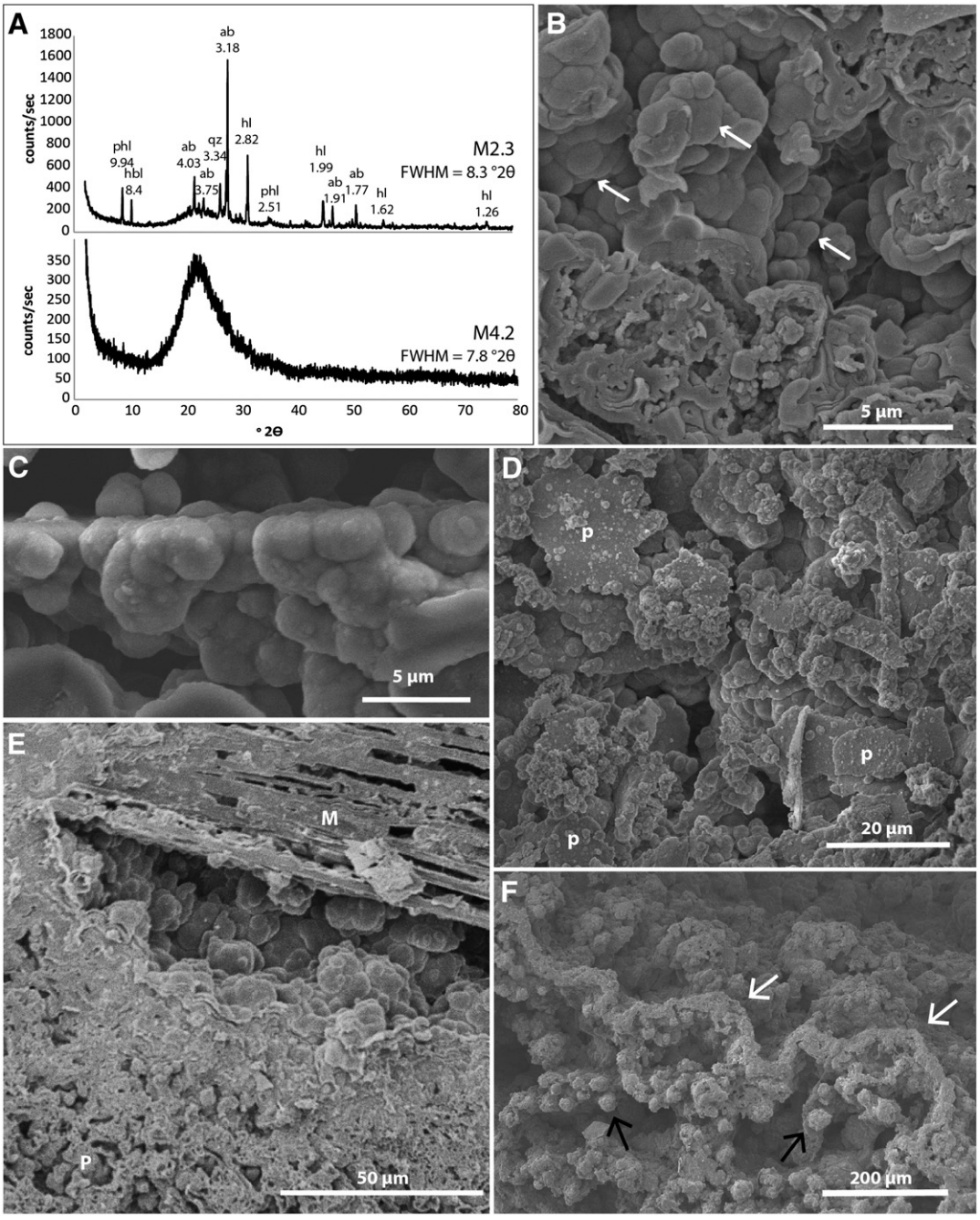

Fig. 5. White sinters: mineralogy, morphology of the silica phase and micro-textures. A: XRD traces of representative samples. The broadband centered at 22.5 °2 for sample M2.3 and 22.4 °2 for sample M4.2 correspond to opal-A. Additional peaks are labeled according to the mineral that they correspond to, and the d-spacing value of each peak, where phl = plogopite, hbl = hornblende, hl = halite and ab = albite. The FWHM value is provided for each sample. Note the difference in the vertical scale between the two XRD traces shown. B: Coalesced smooth opal-A nano- and micro-spheres. C: Bumpy opal-A micro-spheres forming individual laminae. D: Silica platelets deposited pseudo-horizontally in the uppermost sinter surface at site 2. E: Overview of massive (M) and porous (P) silica layers. Massive thin silica laminations also show porosity due to abundant voids. F: Site 4 sinter column surface showing micro columns (black arrows) and ridges (white arrows).

spacings), quartz (with peaks corresponding to 3.34 and 1.81) and plagioclase (possibly albite with 4.03 and 3.18 peaks). These minerals were also observed in between the silica laminations under the petrographic microscope.

Cahnite (Fig. 8 C), a rare arsenic borate ($Ca_4B_2As_2O_{12}{\cdot}4H_2O$), is detected by both XRD and SEM in the colored sinter samples. The XRD peaks correspond to 5.02, 4.67, 3.55, 2.82, 2.62 and 1.82 d-spacings. Cahnite forms tetrahedral crystals frequently twinned that are found filling cavities in sinter from site 6 and forming continuous laminations in site 3 (Fig. 8 D). The infill of sinter cavities at site 6 consists of cahnite crystals and needle-shaped crystals which could not be identified (Fig. 8 D, E). These needle-like crystals correspond to nanometer-scale, elongated crystals that are mainly composed of Si (27 %wt.), Ca (8 %wt.) and As (8 %wt.). The sinter deposit at site 3 is composed by red porous and friable horizons interlayered with white sinter laminations. The red material is composed of flower-like crystals (Fig. 8 F), which mainly consists of As (21 %wt.), Si (17 %wt.) and Fe (16 %wt.), although they have detectable amounts of Mg (5 %wt.), Ca (8 %wt.) and Al (4 %wt.).

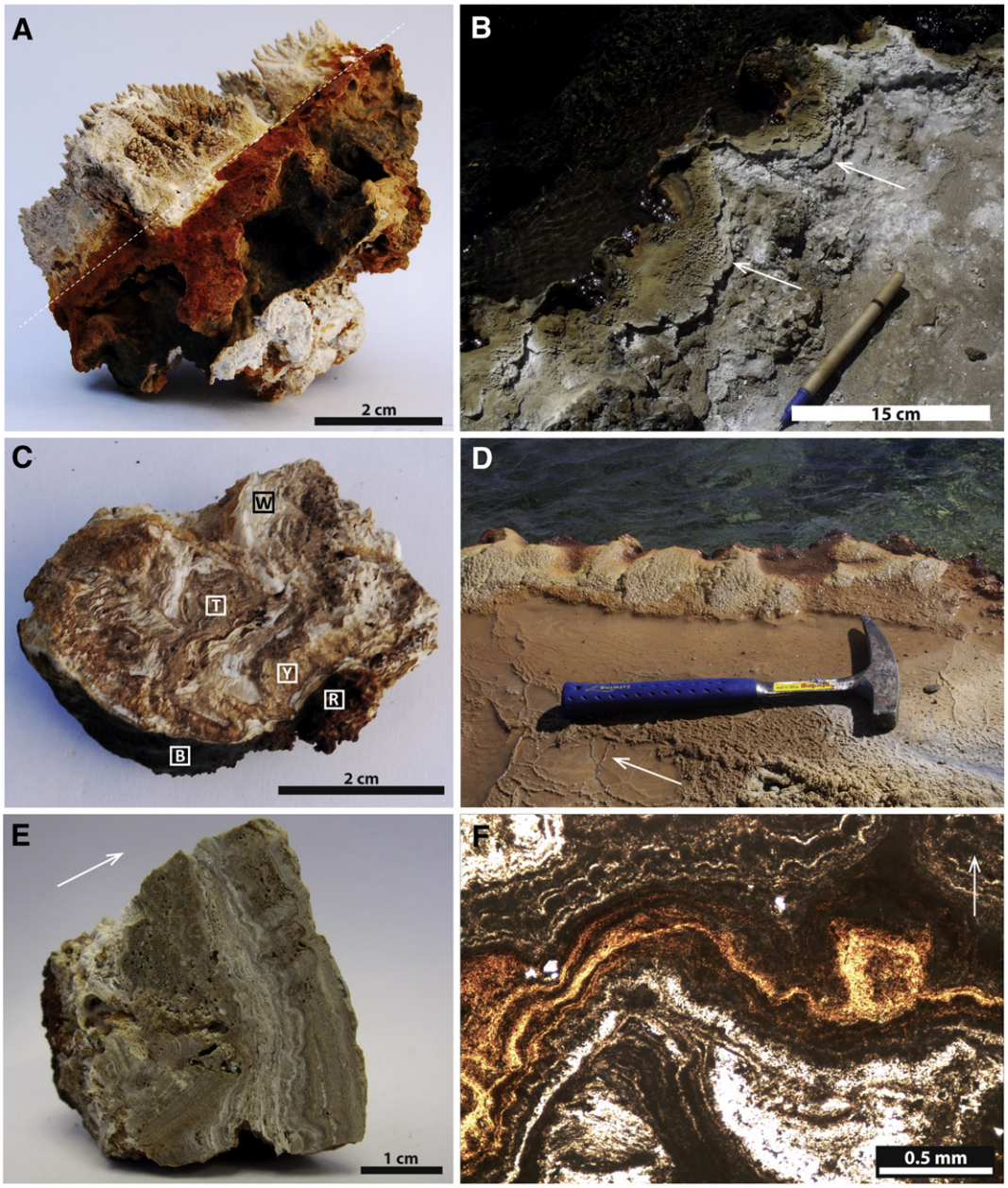

Fig. 6. Colored sinters: macroscopic characteristics and sampling sites. A: Columnar sinter showing a red coloration at the water-air interface (dotted line) and corresponds to a sinter island at the beginning of the discharge channel at site 3. B: Sinter around a hot pool (~82 °C water), with splash texture on pool rim (arrows). C: Internal structure of a colored sinter sample with white (W), tan (T) and yellow (Y) lamminations, site 6. Red (R) and black (B) crusts are found at the water-air interface and sub-aqueous surfaces respectively. D: Sinter pool rim with columnar splash texture around a vigorously boiling and bubbling pool, site 6. Terracettes form in overflow areas (arrow). E: Internal structure of site 6 sinter with seudo-horizontal white and tan laminations. F: White, brown and red laminations of the sample from E under the petrographic microscope.

5.3. Biotic components of El Tatio sinters

Abundant biological material is identified through SEM observation of El Tatio sinters; silicified microorganisms usually correspond to microbial filaments of variable diameter (Fig. 9 A, B, C, D), although diatoms were also found. Diatom-rich horizons occur only at site 6 (Fig. 9 E). Plant material is relatively common and occurs at sites 3, 4 and 6 (Fig. 9 F), whereas silicified pollen particles are found in sinter laminations and columns of sites 3 and 4 (Fig. 9 G).

The occurrence of silicified microbes and other biotic components in El Tatio sinter samples is detailed in Table 4. High- to mid-temperature microbial filaments of <4 μm diameter occur randomly oriented, forming networks in massive and porous silica laminations at all the sampling sites (Fig. 9 B). Low-temperature microbial filaments of >5 μm diameter were identified at site 3, where they are aligned parallel to each other (Fig. 9 D). In particular, ~1 μm diameter microbes were observed at the surface of sinter columns and within sinter laminations of columnar sinter at sites 3 and 5 (Fig. 9 B, C).

5.4. Silica precipitation rate

The environmental conditions at site 3 (silica precipitation rate experiment site) are summarized in Table 5 and were measured the beginning of the *in situ* silica precipitation rate experiment. The wind direction was predominantly east, wind speed varies between 3.7 and 7.5 $m \cdot s^{-1}$ and the average evaporation rate was 0.46 mm/min.

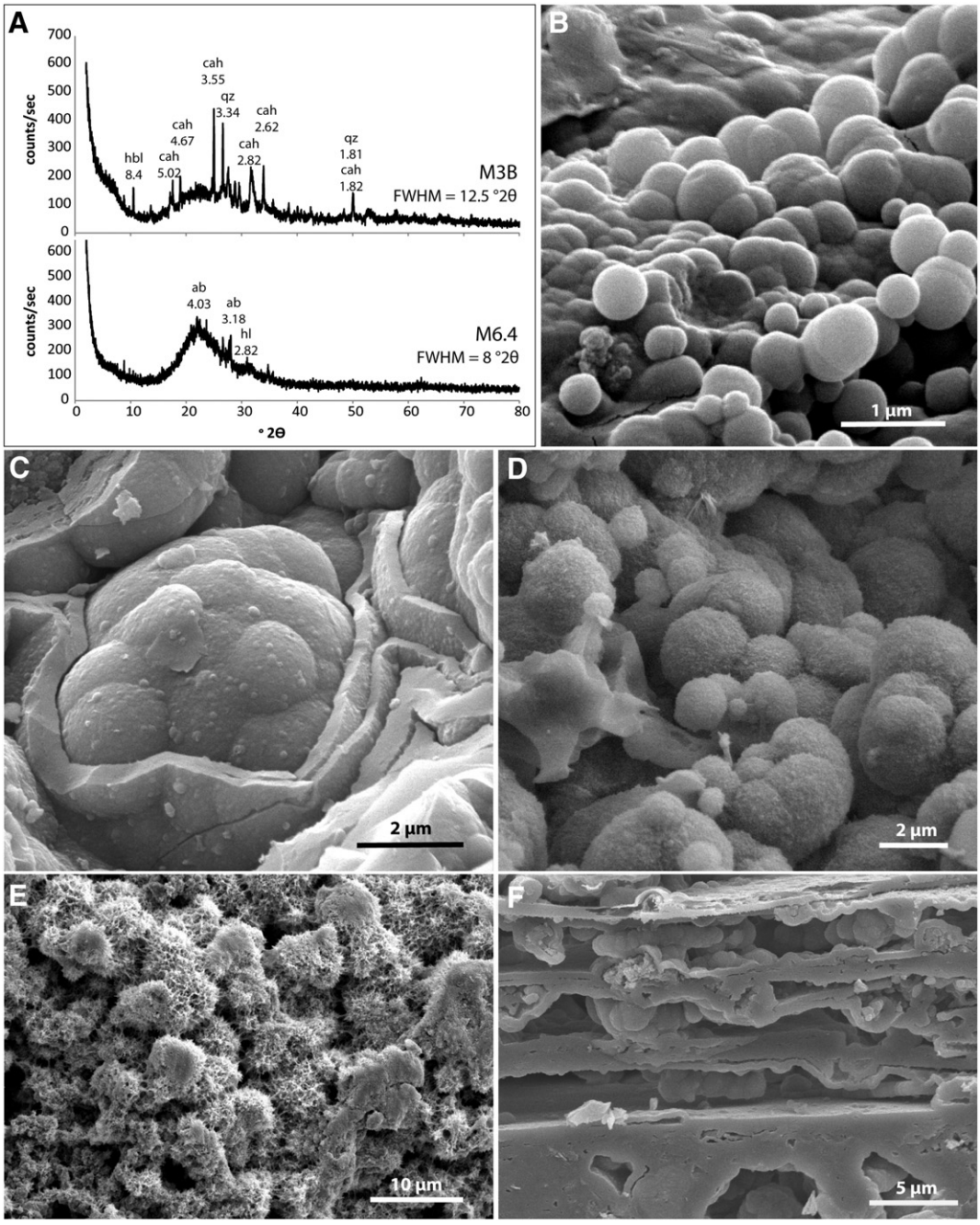

Fig. 7. Colored sinters: mineralogy, morphology of the silica phase and micro-textures. A: XRD traces of representative samples. The broadband centered at 23.7 °2 for sample M3B and 22.8 °2 for sample M6.4 correspond to opal-A. Additional peaks are labeled according to the mineral that they correspond to, and the d-spacing value of each peak, where cah = cahnite, hbl = hornblende, qz = quartz and ab = albite. The FWHM value is provided for each sample. Note the difference in the vertical scale between the two XRD traces shown. B: Smooth opal-A, nano- and micro-spheres. C: Aggregated, opal-A micro-spheres. D: Rough, opal-A micro-spheres from a sinter sample from site 6. E: Spiky micro-spheres from sinter at site 6. F: Massive and porous silica layers from sinter at site 3.

This experiment shows that silica precipitation rate varies depending of the distance between the pool and the slides, their orientation respect to the water flow, and the month of collection, as shown in Fig. 10. According to our results, the average silica precipitation rate at El Tatio is 0.86 mg/day per slide, considering both parallel and perpendicular slides, which equals 0.63 kg/year per m^2 considering that the precipitation area in the slides is 125 mm^2. However, the silica precipitation rate is higher in slides that are placed perpendicular to the water flow (1.17 mg/day per slide, in average) than in those set parallel to it (0.46 mg/day per slide, in average).There is no clear trend between amount of silica precipitated and the month of collection (i.e. the duration of the experiment).

6. Discussion

6.1. Physico-chemical controls on silica precipitation at El Tatio

The El Tatio sinters show a low to extremely low degree of structural order, evidenced by the high FWHM values (7.8–12.5 °2) in XRD data (Table 3). These high FWHM values are expected, as the samples are mainly formed by the least mature silica phase, opal-A, which forms micro-to-nanoscale spheres and aggregates. Nevertheless, the FWHM values of the El Tatio sinter samples are commonly higher than those typically reported for opal-A-bearing sinters from Opal Mound in the US (6.45–7.95 °2), and from Orakei Korako (6.25–8 °2) and Te Kopia

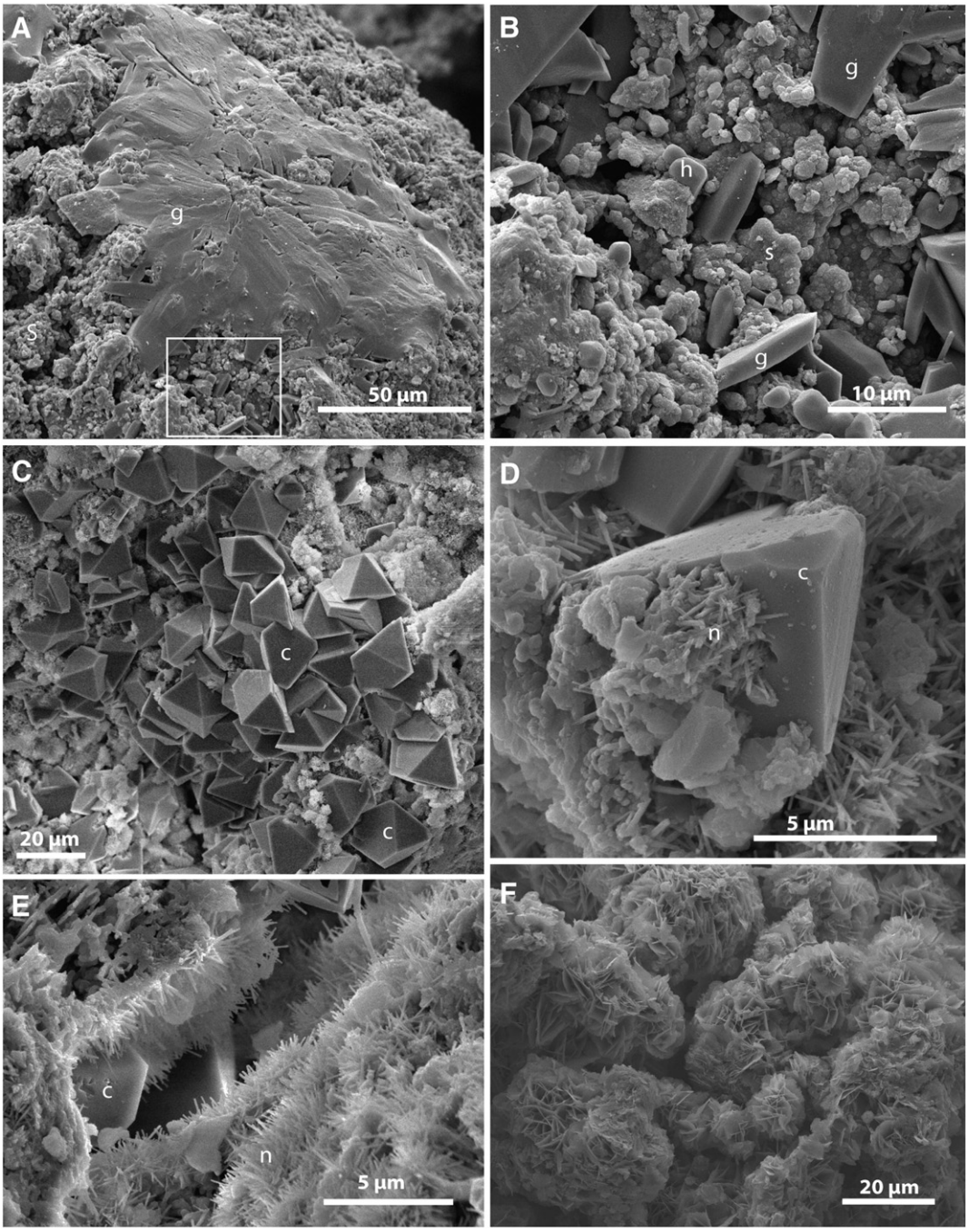

Fig. 8. El Tatio sinter accessory mineralogy. A: Gypsum crystals (g) at the top of a sinter column from a near-vent setting of site 3. The white square shows the location of the image B. B: Close-up of gypsum crystals (g), halite crystals (h) and opal-A spheres (s). C: Tetrahedral and octahedral cahnite crystals (c) form a continuous horizon in a column from a near-vent setting of site 3. D: Tetrahedral cahnite (c) and acicular needle-like crystals (n) in a cavity of sinter from site 6. E: Needle-like crystals (n) and cahnite crystals (c) as secondary infill in a sinter cavity, site 6. F: Flower-like crystals that constitue the red friable laminations from a near vent-sample, site 3.

(5.65–7.25 °2) in New Zealand (Lynne and Campbell, 2003, 2004; Lynne et al., 2005). A previously published mineralogical study by García-Valles et al. (2008) reported high FWHM values (up to 10.5 °2) for halite- and sylvite-rich sinters from El Tatio. The aforementioned authors suggested that FWHM values are increased by the simultaneous occurrence of accessory minerals along with the silica phases. Our mineralogical data of El Tatio sinters, showing high FWHM values and abundant accessory minerals, are in agreement with García-Valles et al. (2008). However, we suggest that there may be a relation between the chemistry of sinter deposits and their degree of structural disorder evidenced by high FWHM values. This hypothesis is supported by our SEM–EDS analyses that show wt% levels of Ca and Na in opal-A microspheres, and by data published by Handley et al. (2005), in which opal-A sinters show FWHM values of 8.9 °2 and concurrently EDS analysis of silica phases detect minor amounts Al, Na and Ca.

Nevertheless, the incorporation of these elements into the silica structure in the form of adsorbed cations acting as bridging ions between silica particles would enhance the structural order of the silica network (Iler, 1979). Thus, we suggest that high structural disorder in El Tatio sinters may be related to the presence of cations attached to internal silanol (Si–OH) groups inside the silica network, since it has been documented that impurities, such as Na, K, or Al, can be occluded inside

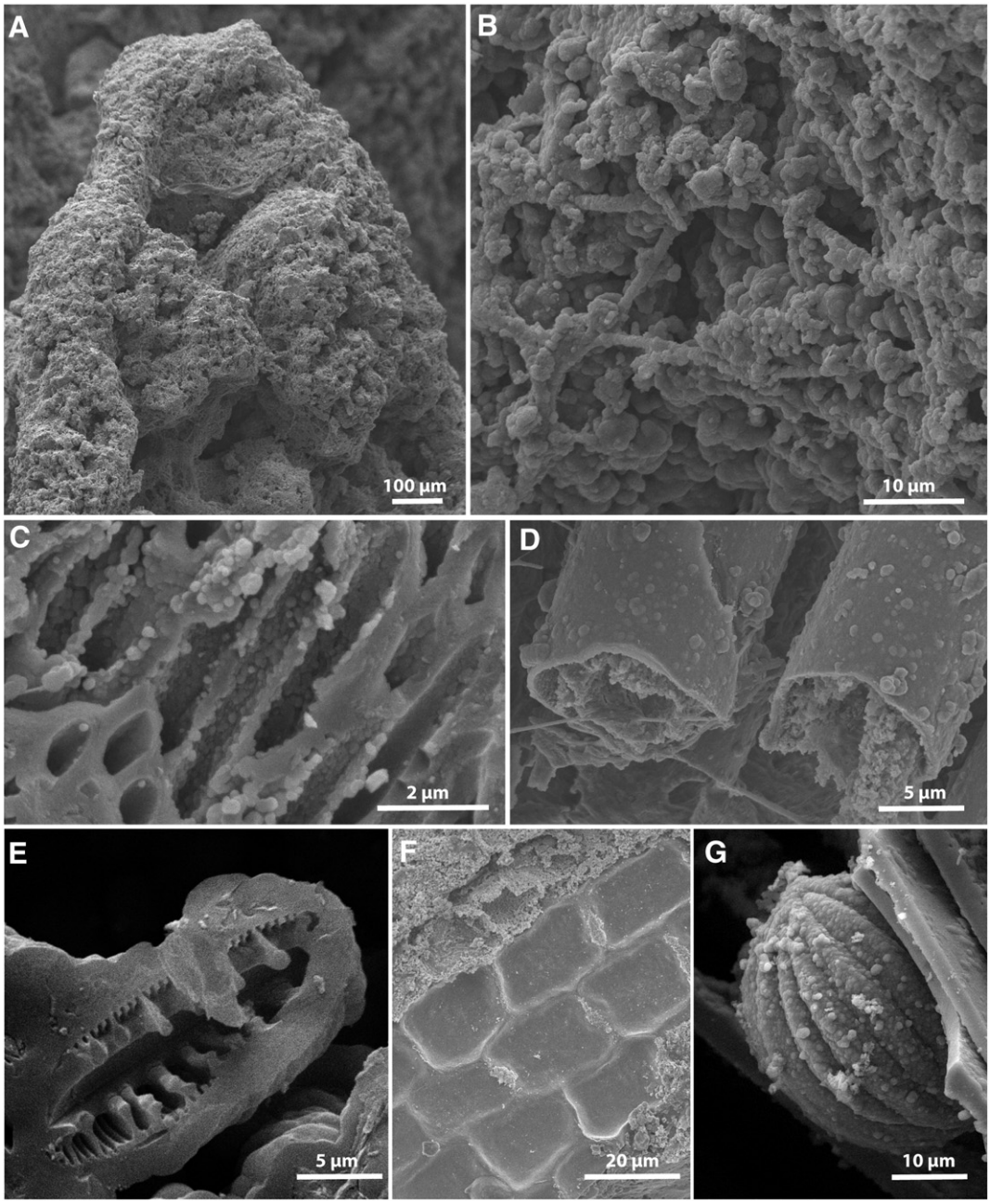

Fig. 9. Microbial components of El Tatio sinters. A: Microbial filaments at the surface of a micro-column, site 3. B: Close-up to ~1.5 µm diameter microbial filaments from (A). C: <1 µm diameter microbial filaments from sample M3.2, site 3. D: >5 µm diameter microbial filaments from sample M3.2, site 3. E: Diatom found at a diatom-rich lamination from sample M6.4, site 6. F: Plant cell casts from sample M3.2. G: Pollen spore between massive silica layers from sample M5, site 5.

the colloidal particles, taking the place of the silanol protons (as with sodium or potassium) or forming isomorphic tetrahedra with an extra negative valence on the surface or inside the particles (Bergna and Roberts, 2005). Another possible explanation for high FWHM values in El Tatio sinter samples consist in the occurrence of nano- to micro-scale minerals or non-crystalline varieties of other minerals, which can cause a superposition of the broadbands of opal-A and broadbands of these other minerals (Fig. 7 A).

However, there are some samples that show the typical opal-A FWHM values (7.8, 7.9 and 8.0 °2 ; Table 3), which may be related to the occurrence of bumpy microspheres silica morphology. Bumpy spheres morphology has been documented in Opal Mound, Sinter Island

Table 5
Environmental conditions at the site of the silica precipitation experiment (site 3).

Position	Distance from pool (m)	Water flow (m/s)	Humidity(%)	Wind velocity (m/s)	Water temperature (°C)
P1	0.74	0.0025	64.2–89	3.7–6.3	72.4
P2	3.24	0.0039	124	5.1–7.2	66.2
P3	6.84	0.0021	88.9–111.7	3.4–6.1	62.7
P4	9.84	0.0024	32–45.2	4.8–7.5	57.4

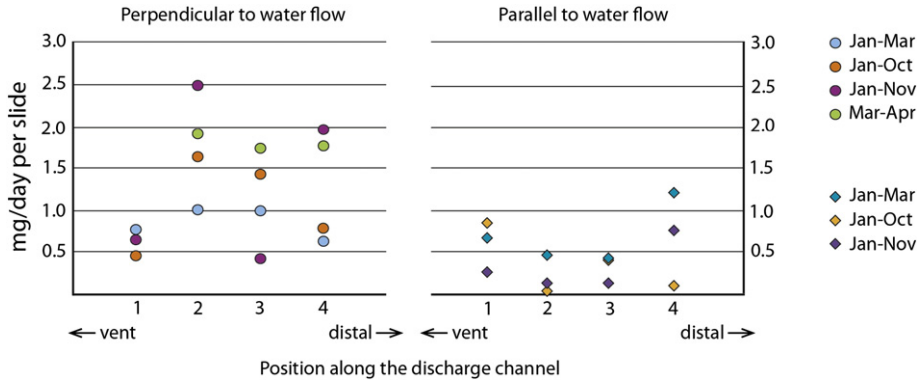

Fig. 10. Silica precipitation rate for the different samples placed at the four positions along the site of experiment discharge channel. Right and left vertical axes are in the same units. Samples are labeled according to the month of their placement in site and the month of collection.

and Steamboat Springs sinters (Lynne et al., 2007). It has been interpreted to correspond to the previous step before opal-A/CT in the diagenetic transformations from opal-A to quartz (Lynne et al., 2007). Thus, bumpy microspheres of El Tatio sinters more likely correspond to a transitional phase between opal-A and opal-A/CT, which would be a slightly more advanced maturation state. The common occurrence of this silica morphology in the mentioned samples is probably linked with their lower the FWHM values.

Apart from smooth opal-A spheres, El Tatio sinters are composed of rough and spiky spheres (Fig. 7 D, E). These silica morphologies are not related to silica phase maturation, because the FWHM values of those sinter samples are high (8.0 °2 and 12.5 °2). Conversely, they are remarkably similar to the "silica stars" reported by Campbell and Lynne (2006) in sinters from Sinter Island, New Zealand. The "silica stars" morphology has been interpreted to form by dissolution produced as a result of acid fluid circulation through the sinter deposit (Campbell and

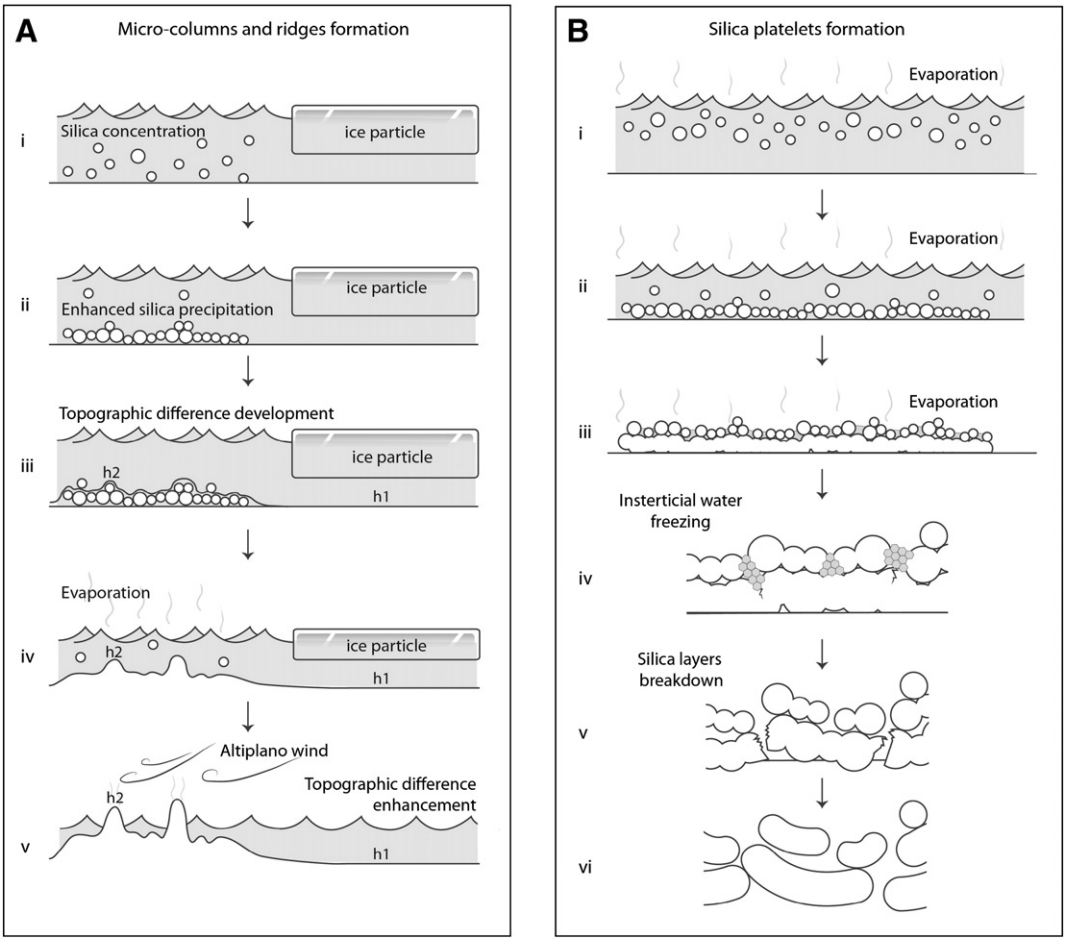

Fig. 11. Formation of freezing-related sinter textures at El Tatio. A: Micro columns and ridges formation is influenced by an increased precipitation rate in the surroundings of an ice particle (i–ii). This higher precipitation rate enhances the development of a topographically-high zone (h2) and a topographically-low zone (h1) (iii). There is higher evaporation in topographically high zones, which increments the topographic contrast, due to the effect of high evaporation rates at El Tatio and the Altiplano wind (iv–v). B: Silica platelets formation begins with the silica nucleation and precipitation to form an individual silica layers (i–iii). Freezing conditions may produce freezing of interstitial water between the recently formed silica particles, increasing its volume and therefore fracturing the silica layer (iv–vi).

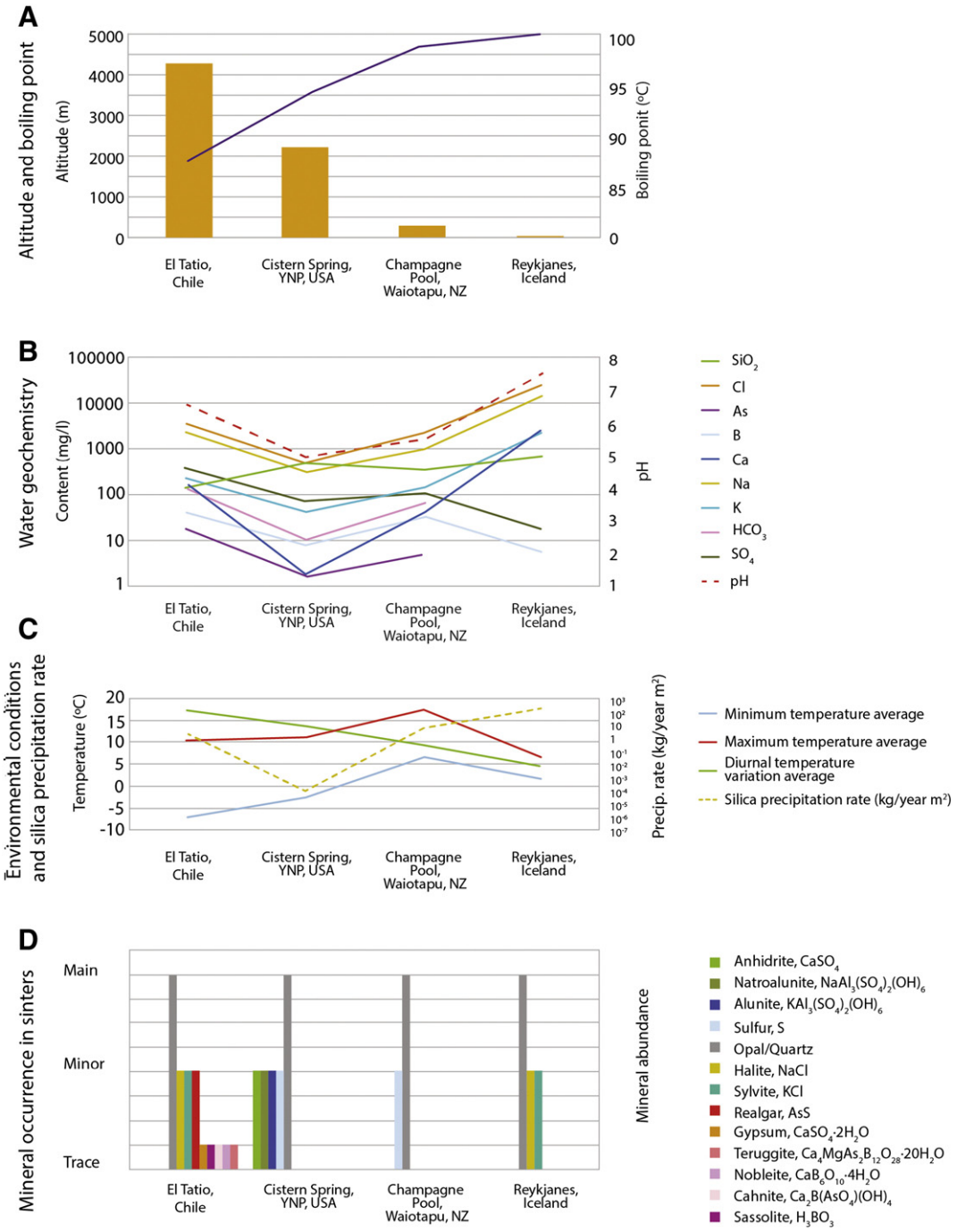

Fig. 12. Comparison between El Tatio and other sinter bearing systems. Mineralogy, water geochemistry and silica precipitation data from Cistern Spring, Champagne Pool and Reykjanes from: Rodgers et al., 2002a; Guidry and Chafetz, 2003; Pope et al., 2004; García-Valles et al., 2008; Tobler et al., 2008; Handley et al., ; White et al., 1988. Environmental conditions at Champagne Pool were taken from NIWA database: New Zealand Institute of Water and Atmospheric Research air temperature data presented here as average of the hourly temperatures of Taupo AWS station from 2000 to 2004. Environmental conditions at El Tatio were taken from DGA database: data from Dirección General de Aguas daily maximum and minimum temperatures at El Tatio station from 2000 to 2004. Environmental conditions at Reykjanes correspond to daily maximum and minimum temperatures at Reykiavik weather station from 1961 to 1990. Environmental conditions at Yellowstone National Park taken from the Western Regional Climate Center.

Lynne, 2006). Additionally, in El Tatio sinters, rough and spiky spheres co-exist with flower-like crystals (Fig. 8 F), which may correspond to smectite-like clays. Smectite commonly forms in acidic conditions (pH 4–6; Corbett and Leach, 1998), which support the idea that acid fluid circulation produced dissolution in El Tatio sinters.

The mineralogy of El Tatio sinters also include other mineral phases such as halite, gypsum, cahnite ($Ca_4B_2As_2O_{12}{\cdot}4H_2O$) and other unidentified Ca–As–Fe-rich minerals (needle-like and flower-like crystals; Fig. 8). In particular, the presence of cahnite in the El Tatio sinters has not been previously reported, but it is not surprising, as other arsenic minerals such as teruggite ($Ca_4MgAs_2B_{12}O_{28} \cdot 20H_2O$) and nobleite ($CaB_6O_{10} \cdot 4H_2O$) have been documented at El Tatio (Rodgers et al., 2002a; García-Valles et al., 2008). The precipitation of these minerals reflects the particular geochemistry of hot springs at El Tatio, which is characterized by high contents of Na, Cl, Ca, As, B (Table 1). However, the sinter deposits around the group of less diluted thermal springs does not show higher content of accessory minerals. This indicates that there is no direct relation between the concentration of these elements in the currently discharging thermal waters and the abundance of halite, gypsum and cahnite in the sinter

deposit. The difference between the water and sinter chemistry may be explained in part because some sites do not reach full evaporation states, necessary for the precipitation of these highly soluble minerals, and thus, elements such as Na, Ca, B and As largely remain in the fluid phase. The observed reddish coloration of the analyzed sinter samples is probably linked to the occurrence of Ca–As–Fe-rich flower-like crystals between the silica layers, as they constitute the red porous friable laminations of sample M3B and they are also present more diffusely in sample M6.4.

XRD analyses of El Tatio sinter samples evidence the presence of micas, amphiboles, quartz and plagioclase. However, it is very likely that these minerals correspond to detrital fragments blown into the sinter deposit by the wind from the surrounding volcanic rocks.

Few studies have addressed the issue of sinter accumulation rate, some have focused on theoretical modelling (e.g., Boudreau and Lynne, 2012) and others use an experimental approach (Handley et al., 2005; Tobler et al., 2008). In situ silica accumulation experiments have been developed at Champagne Pool (pH = 5.5; T = 75 °C; 362 mg/l SiO_2; Pope et al., 2004), Waiotapu in New Zealand where sub-aerial silica precipitation occur at a rate of 0.2 to 1.9 mg/day per slide (=1 to 10 kg/year per m^2; Handley et al., 2005), and at Reykjanes and Svartsegi in Iceland (pH ~ 7; T = 42–75 °C; 250–695 mg/l SiO_2) where sub-aqueous precipitation rate ranges from 10 to 304 kg/year per m^2 (Tobler et al., 2008). The experimental *in situ* silica precipitation data obtained for the El Tatio indicate that sinter precipitates mostly sub-aerially, which agrees with water being undersaturated with respect to silica at all sites. The experimental precipitation rate at El Tatio is 1.34 to 3.4 kg/year per m^2. The sinter precipitation rate at El Tatio is probably increased by the incorporation of cations into the silica structure (Iler, 1979), and the high evaporation rate due to: (1) the frequent and strong winds of the Altiplano and/or (2) the high cooling rate of thermal water due to low air temperature. The main controls on water evaporation rate correspond to water temperature and how air humidity is less important (Boudreau and Lynne, 2012). At high altitude in the Altiplano, winds are usually very strong and it might be the main environmental condition controlling the evaporation rate at El Tatio. The obtained precipitation rates are relatively high (average 0.86 mg/day per slide = 0.63 kg/year per m^2) considering that the silica content in the thermal water is considerably lower (147 SiO_2 ppm) than that of the other silica precipitation sites such as Champagne Pool at Waiotapu, in New Zealand, and Reykjanes, in Iceland.

The silica precipitation rate is significantly higher in slides that are placed perpendicular to the water flow (1.17 mg/day per slide) than in those set parallel to it (0.46 mg/day per slide). Moreover, in perpendicular slides, the side facing the thermal pool shows thicker silica crusts than the side towards the water flow. Perpendicular slides offer more resistance to water low, which causes high amplitude waves to form immediately next to the slide on the side facing the thermal pool. These waves supply the silica that is precipitated on the slide.

It was expected that silica precipitation would be higher in near vent locations (closer to the thermal pool, in positions 1 and 2) and lower in distal locations (positions 3 and 4). However, there is no clear trend between the precipitation rate and the position along the channel. In some samples, it appears to be a lower precipitation rate at position 1 in both parallel and perpendicular slides, compared to the rest of the positions. This might be related to the effect of lower amplitude waves in this position compared to distal locations. High precipitation rates are also registered in the most distal position along the channel (position 4); this is more likely caused by the abundant presence of microbial mats (orange-red colored areas in Fig. 2B), which enhance the precipitation rate. This process has been described by several authors who propose that biotic components in thermal springs can provide reactive sites for biologically passive silica precipitation (Konhauser and Ferris, 1996; Farmer, 1999; Phoenix et al., 2000; Benning et al., 2004). There is no clear trend between the month of collection and the experimental precipitation rate obtained, which can be related to unmeasured erosion effects. Thus the obtained silica precipitation rates for El Tatio correspond to a minimum estimation.

Based on our experimental data, a rough estimation can be done of the time that would be necessary to form the large siliceous sinter deposits at El Tatio. Since silica precipitation rate varies with distance from the vent, we used a minimum and maximum approach for this calculation. The average precipitation rate for slides parallel to the water flow represents the minimum (0.46 mg/day per slide = 1.34 kg/year per m^2) and the average precipitation rate for slides perpendicular to water flow represents the maximum precipitation (1.17 mg/day per slide = 3.4 kg/year per m^2). Considering that opal-A siliceous sinters have an average density of 1.8 g/cm^3 (Herdianita et al., 2000), and that at El Tatio the sinter deposits cover approximately 2 km by 0.5 km (Fig. 2) with an average depth of 1 m, based on outcrops field observations, approximately ~6000 kg/m^2 of sinter mass occurs at El Tatio. Assuming that the experimentally-determined precipitation rate was constant through time, then the El Tatio sinters would have begun to form between ~1500 and ~4000 years ago. These two ages correspond to the maximum and minimum age calculated based on the maximum and minimum precipitation rates experimentally obtained. In the absence of direct (absolute) age information, and despite the fact that this calculation has many uncertainties (e.g., under/overestimation of the actual amount of silica, variations of precipitation rates over time, effects of sub-aqueous precipitation and erosion/dissolution effects), these ages provide an approximate constraint on the recent (post-Pleistocene) activity at the El Tatio geothermal field. However, the observed silicification of plant material indicates that carbon dating could be performed to obtain absolute ages for El Tatio sinters.

6.2. Environmental implications

The impact on silica precipitation under El Tatio's extreme climatic and high-altitude conditions has been scarcely studied. Experimental cryogenic silica precipitation studies have been documented to produce characteristic sinter micro-texture consisting of folded sheets and structurally complex particles that exhibit branching, swellings and are commonly terminated in “tear-drops”, (Channing and Butler, 2007). The same study shows the resemblance of these experimentally produced particles with the textures observed in sinter samples from the Yellowstone National Park, USA, which clearly shows how the hot spring environmental conditions influence silica morphology.

The different micro-textures reported in this study, such as micro-columns/ridges (Fig. 5 F) and silica platelets (Fig. 5 D) occurring in both white and colored sinters, may be linked to silica precipitation under sub-zero temperatures at high altitude (>4200 m above sea level). For example, micro-columns and ridges observed around eruptive pools (Fig. 5 F) may be the result of variations in local precipitation rates related to ice particles. The partial freezing of thermal waters leads to concentration of all dissolved chemical components in the surroundings of the ice particles, as only pure water form ice crystals. This process locally enhances the silica precipitation in the surrounding areas (Channing and Butler, 2007). Furthermore it creates a topographic difference between the surfaces that have ice particles above and those that lack ice. Another environmental feature to consider relates to contrasts in evaporation rates between topographically-high and -low sites. According to Boudreau and Lynne (2012), topographically-high zones will more likely fully evaporate, whereas water may remain at topographically-low sites, between eruptive events. This leads to an enhanced silica precipitation at topographically-high zones due to complete evaporation, which is enhanced by high evaporation rates and the strong winds of the Altiplano. Therefore, the origin of micro-column and ridge textures at El Tatio is most likely the result of a combination of both processes. The presence of ice particles in the cooled thermal water favors silica nucleation generating minor topographic highs that are more likely to reach complete evaporation, enhancing their growth (Fig. 11 A).

Silica platelet textures observed at El Tatio (Fig. 5 D) also suggest that daily fluctuations in temperature may have an unforeseen impact on sinter formation in high-altitude systems, where significant atmospheric oscillation leads to night-day freezing-unfreezing cycles. Freezing would lead to an increase in the volume of interstitial water remaining in newly-formed silica layers, which can cause the breakdown of the silica layer. The breakdown of the initial silica layer forms the silica platelets. As day temperatures rises enough to allow thawing to take place, silica platelets may dislocate, producing the observed texture (Fig. 11 B). Similar features have been previously described by Iler (1979), who documented "sheet or flake-like amorphous silica particles" formed by freezing of silica-rich solutions. The formation of ice crystals induce the polymerization of colloidal silica in the solution surrounding the ice particles, leading to the formation of irregular-shaped silica flakes between the flat surfaces of ice crystals (Iler, 1979). However, it is important to note that these experimentally-produced "silica flakes" are 20–30 Å in diameter, and thus, are considerably smaller than the 15–30 μm diameter silica platelets identified in El Tatio sinters.

It has been widely documented that sinter deposits contain abundant remnants of silicified microbial filaments (e.g., Konhauser et al., 2001; Lynne and Campbell, 2003; Jones et al., 2004). The biotic features of sinters are important for studies related to extremophilic life on Earth and the Solar System (e.g. Farmer, 1998; Farmer and Des Marais, 1999; Farmer, 2000; Westall et al., 2001; Konhauser et al., 2003). Also their study in geothermal areas has been proven to be useful for determining paleo-environmental conditions (e.g., Lynne, 2012). It is widely documented that ~1 μm diameter microbes thrive in high temperature water (>60 °C) and are found in near-vent settings, while low temperature > 5 μm diameter microbes are found in the distal parts of hot-spring aprons where the water temperature is < 35°C (e.g., Pierson and Castenholz, 1974; Cady and Farmer, 1996; Hinman and Lindstrom, 1996; Walter et al., 1996; Jones et al., 1997b; Walter et al., 1998; Farmer, 2000; Campbell et al., 2001; Lynne and Campbell, 2003; Lynne, 2012). At El Tatio, we found a variety of microbes and other biotic components preserved in the sinter deposits (Fig. 9). In particular, we found the co-existence of microbial filaments of variable diameter in the same setting (Table 4; Fig. 9).The occurrence of ~1 and 10 μm diameter microbes in the same sinter sample at El Tatio may reflect variations in water temperature through time. For recent times, there is evidence of an increase in the fluid temperature in site 3, as the ~1 μm diameter microbes were found at the sinter surface. It is possible that these particular low- and high-temperature microbes have adapted to the variations in water temperature which has been suggested by Franks (2012) at El Tatio.

Additionally, at El Tatio high-temperature sinter texture (columnar) and preserved mid-temperature microbial filaments co-exist (sample M3B; Fig. 9 A, B). In this case, the sinter sample was taken from a near-vent area of site 3, where the pool temperature ranges from 82 to 84 °C and the up-flow is usually calm with minor eruptive events and intermittent overflowing. The occurrence of low-temperature microbes in high-temperature, near-vent environments has been reported in geothermal areas of New Zealand (Jones et al., 1997a, 2003). This situation has been explained by microbial growth that was restricted to near-vent areas that were only temporarily or not directly in contact with high-temperature or boiling water (Jones et al., 1997a, 2003). It is also probable that at El Tatio, the decreased boiling point at high altitude (86 °C at 4200 m a.s.l.) and the low ambient temperature (average 8–11 °C during the day, and reaching −30 °C at night; Fernandez-Turiel et al., 2005), allow the erupting water droplets to cool fast enough before they land over the sinter deposit that mid-temperature microbes can live in near-vent areas. Additionally, the eruptive events of this particular site may be very infrequent, allowing the colonization of mid-temperature microbes.

The interaction between microbial communities and the hot springs they thrive in, remains a complex interplay of multiple factors (e.g., water temperature and chemistry, amount of flow, altitude, climate). The pristine microbial preservation within siliceous sinters at El Tatio provided an ideal geothermal setting to further explore these inter-relationships.

6.3. Comparison between El Tatio and other sinter bearing systems

El Tatio sinters can be considered unique due to three characteristics: (1) it is located at >4000 m above sea level, and exposed to extreme environmental conditions, such as high daily air temperature oscillation and strong winds; (2) they present freezing-related textures such as silica platelets and micro columns and ridges; and (3) accessory mineralogy includes rare and very soluble arsenic and boron minerals that precipitate by full evaporation of boron and arsenic-enriched waters.

This section presents similarities and differences between El Tatio and three selected sinter bearing systems located at various altitudes: Cistern spring in Yellowstone National Park, in USA (2250 m a. s. l.); Champagne Pool, in New Zealand (304 m a. s. l.); and Reykjanes wastewater drain, in Iceland (40 m a. s. l.; Fig. 12 A). It can be noticed that the silica precipitation rate at El Tatio is higher than that of Cistern Spring and similar to that of Champagne Pool, even though the silica content of El Tatio waters is the lowest (Fig. 12 B, C). This suggests that environmental conditions play an important role in the silica precipitation rate, independent from the probable enhancing effect of cation incorporation into the silica structure, as previously discussed. High diurnal environmental temperature variation and low minimum temperatures allow freezing and thawing to take place at El Tatio, producing the described freezing-related textures. It can be hypothesized that silica platelet textures can also be present in other sinter bearing systems where environmental temperatures allow freezing and thawing events in short time periods, but will be absent in locations where cold conditions are persistent, such as Reykjanes in Iceland, and in warmer regions such as Taupo in New Zealand. In fact, freezing-related textures occur in sinters from Yellowstone National Park in USA, where there is also high diurnal temperature variation (Fig. 12 C; Channing and Butler, 2007).

Additionally, the particular geochemistry of thermal waters seems to be correlated with accessory mineralogy in sinters. Arsenic and boron content of El Tatio waters is higher that of Cistern Spring, Champagne Pool, and Reykjanes, and boron and arsenic minerals: cahnite, sassolite, nobleite, and teruggite. Potassium and calcium content of El Tatio and Reykjanes are the highest, and also these sites present potassium and sodium salts: halite and sylvite (Fig. 12. D).

7. Conclusions

The study of thermal water and associated sinter deposits at the El Tatio geothermal field in northern Chile provides new insights into the characteristics of siliceous sinters formed in an Andean setting characterized by high altitude, high evaporation rates and great air temperature variability.

El Tatio geothermal field show extensive siliceous sinter deposits, which are the result of silica precipitation from near-neutral thermal waters with a SiO_2 concentration of 147–285 mg/l. Arsenic and boron are also present in relatively high concentration compared to other geothermal systems (Fig. 12). This particular water chemistry at El Tatio is reflected in the mineralogy of sinter deposits. Crystalline phases are commonly incorporated into the El Tatio sinters, especially halite and gypsum. Calcium and iron/arsenic-rich minerals, some of which correspond to cahnite, are found filling cavities and constituting laminations within the sinter deposits. Their occurrence in the sinter deposits is possibly linked to the coloration of the sinters and reflects the full evaporation of high-sodium, sulfur, arsenic and boron thermal waters.

The siliceous sinters at El Tatio are mainly constituted by micro- and nano-scale opal-A spheres, and show FWHM values that are among the

highest reported for sinters (7.8 to 12.5 ° 2). The high structural disorder of silica from El Tatio is interpreted to be related to the incorporation of metal cations in the silica structure and the inclusion of micro-to-nano scale phases such as cahnite and/or clay minerals. The high content of cations such as Ca and Na in the thermal waters is strongly tied to high silica precipitation rates, estimated in 2.5 kg/m^2 per year based on *in situ* precipitation experiments. The particular environmental conditions of this high-altitude geothermal area, such as windy conditions and low atmospheric pressure, may also be responsible for rapid silica precipitation.

Environmental conditions such as freezing and low boiling point have an impact on sinter textures, as distinctive macro- and micro-textures were identified in the El Tatio sinters. Silica platelet formation is attributed to freezing–unfreezing events that occur daily at El Tatio, as sub-zero temperature is common at night, while day temperatures usually rises enough for thawing to take place. Micro-columns and ridges are interpreted to form due to an enhanced local precipitation rates related to silica concentration near ice particles.

Microbial textures are also common in El Tatio sinters, as is in most studied sinters in USA and New Zealand (e.g., Braunstein and Lowe, 2001; Konhauser et al., 2001; Lynne and Campbell, 2003; Mountain et al., 2003; Smith et al., 2003; Jones et al., 2004). Yet, the co-existence of columnar texture with mid-temperature microbial filaments is an interesting finding, because columnar texture is commonly related to eruptive, near-vent high-temperature settings (e.g. Lowe and Braunstein, 2003; Lynne, 2012). This situation has been previously documented and explained by microbial growth being restricted to near-vent areas that were only temporarily or not directly in contact with high-temperature or boiling water (Jones et al., 1997a, 2003). Nevertheless, the lower boiling temperature at high-altitude and infrequent eruptive events would also allow the co-existence of boiling-related texture and mid-temperature microbes. Thus, at El Tatio and other high-altitude geothermal fields, the interpretation of historic near-vent settings would be more accurately achieved if based on sinter textures (i.e., splash textures) rather than on the characteristics of microbial communities.

Pristine preservation of a wide diversity of microbes and plants at El Tatio makes these sinters ideal for dating. The study of microbiota that thrive in thermal springs can be used to reconstruct paleo hot-spring environments from near-vent to distal-slope settings. Biotic and abiotic sinter textures are commonly used in geothermal exploration to reconstruct paleo-hydrology and to estimate the total heat flow of low-altitude systems (Lynne, 2012). However, this study highlights the complexity of hot spring environments and emphasizes the importance of site specific studies.

In summary, this work comprises mineralogical and textural determinations, along with thermal water characterization and relates them with high altitude conditions, water chemistry and air temperature. The results of this study reveal that the integrative study of siliceous sinters in active geothermal fields helps to understand the impact of environmental conditions, providing new insights about the nature of siliceous sinters in the Andean context.

Acknowledgements

Financial support for this study was provided by FONDAP project 15090013 “Centro de Excelencia en Geotermia de los Andes, CEGA” is acknowledged. Constanza Nicolau thanks CONICYT for providing support through a M. Sc. scholarship (“Programa de Becas de Magíster”). We thank Catherine Hobbis and Christian Nievas from the University of Auckland and Universidad de Chile for their support in obtaining SEM images, and Rubén Yagüe for his help in XRD analyses. We acknowledge Fernanda Álvarez, Fernanda Soto, Pablo Sánchez and Óscar Benavente for their logistic help during fieldwork. We would also like to acknowledge Alan Boudreau and an anonymous reviewer for their valued comments that helped improve this manuscript.

References

Benning, L.G., Phoenix, V.R., Yee, N., Konhauser, K.O., 2004. The dynamics of cyanobacterial silification: an infrared micro-spectroscopic investigation. Geochim. Cosmochim. Acta 68, 743–757.
Bergna, H.E., Roberts, W.O., 2005. Colloidal Silica: Fundamentals and Applications. CRC Press (944 pp.).
Boudreau, A.E., Lynne, B.Y., 2012. The growth of siliceous sinter deposits around high-temperature eruptive hot springs. J. Volcanol. Geotherm. Res. 247–248, 1–8.
Braunstein, D., Lowe, D.R., 2001. Relationship between spring and geyser activity and the deposition and morphology of high temperature (>73 C) siliceous sinter, Yellowstone National Park, Wyoming, U.S.A. J. Sediment. Res. 71, 747–763.
Cady, S.L., Farmer, J.D., 1996. Fossilization processes in siliceous thermal springs: trends in preservation along thermal gradients. In: Bock, G.R., Goode, J.A. (Eds.), Evolution of Hydrothermal Ecosystems on Earth (and Mars?). Proceedings of the CIBA Foundation Symposium, 202. Wiley, Chichester, U.K, pp. 150–173.
Campbell, K.A., Lynne, B.Y., 2006. Diagenesis and dissolution at Sinter Island (453 yrs BP), Taupo Volcanic Zone: Silica stars and the birth of quartz. Proceedings of the 28th New Zealand Geothermal Workshop, Auckland, New Zealand.
Campbell, K.A., Sannazzaro, K., Rodgers, K.A., Herdianita, N.R., Browne, P.R.L., 2001. Sedimentary facies and mineralogy of the Late Pleistocene Umukuri silica sinter, Taupo Volcanic Zone, New Zealand. J. Sediment. Res. 71, 727–746.
Channing, A., Butler, I.B., 2007. Cryogenic opal-A deposition from Yellowstone hot springs. Earth Planet. Sci. Lett. 257, 121–131.
Corbett, G.J., Leach, T.M., 1998. Southwest Pacific gold–copper systems. Structure, alteration and mineralization. Special Publication, 6. Society of Economic Geologists (238 pp.).
Cortecci, G., Boschetti, T., Mussi, M., Herrera Lameli, C., Mucchino, C., Barbieri, M., 2005. New chemical and original isotopic data on waters from El Tatio geothermal field, northern Chile. Geochem. J. 39, 547–571.
Cusicanqui, H., Mahon, W.A.J., Ellis, A.J., 1975. The geochemistry of the El Tatio Geothermal Field, northern Chile. Proceedings, Second United Nations Symposium on the Development and Use of Geothermal Resources, San Francisco, pp. 703–711.
DGA, 2010. Metodología para la estimación de recarga de cuencas altiplánicas y precordilleranas de vertiente pacífica en el norte de Chile, XV, I, II y III Regiones. Ministerio De Obras Públicas, Dirección General de Aguas.
Downs, R.T., Hall-Wallace, M., 2003. The American Mineralogist Crystal Structure Database. Am. Mineral. 88, 247–250.
Farmer, J.D., 1998. Thermophiles, early biosphere evolution and the origin of life on Earth: implications for the exobiological exploration of Mars. J. Geophys. Res. 103, 28457–28461.
Farmer, J.D., 1999. Taphonomic modes in microbial fossilization. Size Limits of Very Small Microorganisms: Proceedings of a Workshop. National Academy Press, Washington DC, pp. 94–102.
Farmer, J.D., 2000. Hydrothermal Systems: doorways to early biosphere evolution. GSA Today 10, 1–9.
Farmer, J.D., Des Marais, D.J., 1999. Exploring for a record of ancient martian life. J. Geophys. Res. 104, 26977–26995.
Fernandez-Turiel, J.L., Garcia-Valles, M., Gimeno-Torrente, D., Saavedra-Alonso, J., Martinez-Manent, S., 2005. The hot spring and geyser sinters of El Tatio, Northern Chile. Sediment. Geol. 180, 125–147.
Fournier, R.O., Rowe, J.J., 1966. Estimation of underground temperatures from the silica content of water from hot springs and steam wells. Am. J. Sci. 264, 685–697.
Franks, M.A., 2012. Archaea at the El Tatio Geyser Field: community composition, diversity, and distribution across hydrothermal features and geochemical gradientsPh. D. Thesis University of Texas, U. S. A (183 pp.).
García-Valles, M., Fernández-Turiel, J.L., Gimeno-Torrente, D., Saavedra-Alonso, J., Martínez-Manent, S., 2008. Mineralogical characterization of silica sinters from the El Tatio geothermal field, Chile. Am. Mineral. 93, 1373–1383.
Giggenbach, W.F., 1978. The isotope composition of waters from the El Tatio geothermal field, northern Chile. Geochim. Cosmochim. Acta 42, 979–988.
Giggenbach, W.F., Gouguel, R.L., 1989. Collection and analysis of geothermal and volcanic water and gas discharges. Department of Scientific and Industrial Research, Chemistry Division, Petone, New Zealand (172 pp.).
Glennon, J.A., Pfaff, R.M., 2003. The extraordinary thermal activity of El Tatio geyser field, Antofagasta Region, Chile. GOSA Trans. 8, 31–78.
Guidry, S.A., Chafetz, H.S., 2003. Depositional facies and diagenetic alteration in a relict siliceous hot spring accumulation: examples from Yellowstone National Park, U.S.A. J. Sediment. Res. 73, 806–823.
Hampton, W.A., White, G.P., Hoskin, P.W.O., Browne, P.R.L., Rodgers, K.A., 2004. Cinnabar, livingstonite, stibnite and pyrite in Pliocene silica sinter from Northland, New Zealand. Mineral. Mag. 68, 191–198.
Handley, K.M., Campbell, K.A., 2011. Character, analysis and preservation of biogenecity in terrestrial siliceous stromatolites from geothermal settings. In: Tewari, V.C., Seckbach, J. (Eds.), Stromatolites: Interaction of Microbes with Sediments, Cellular Origin, Life in Extreme Habitats and, Astrobiology, 18, pp. 359–381.
Handley, K.M., Campbell, K.A., Mountain, B.W., Browne, P.R.L., 2005. Abiotic–biotic controls on the origin and development of spicular sinter: in situ growth experiments, Champagne Pool, Waiotapu, New Zealand. Geobiology 3, 93–114.
Herdianita, N.R., Browne, P.R.L., Rodgers, K.A., Campbell, K.A., 2000. Mineralogical and textural changes accompanying ageing of silica sinter. Mineral. Deposita 35, 48–62.
Hinman, N., Lindstrom, R.F., 1996. Seasonal changes in silica deposition in hot spring systems. Chem. Geol. 132, 237–246.
Iler, R.K., 1979. The chemistry of silica: solubility, polimerization, colloid and surface properties and biochemistry. Wiley, New York (866 pp.).

Jones, B., Renaut, R.W., 1997. Formation of silica oncoids around geysers and hot springs at El Tatio, northern Chile. Sedimentology 44, 287–304.
Jones, B., Renaut, R.W., 2003. Hot spring and geyser sinters: the integrated product of precipitation, replacement and deposition. Can. J. Earth Sci. 40, 1549–1569.
Jones, B., Renaut, R.W., Rosen, M.R., 1997a. Vertical zonation of biota in microstromatolites associated with hot springs, North Island, New Zealand. Palaios 12, 220–236.
Jones, B., Renaut, R.W., Rosen, M.R., 1997b. Biogenicity of silica precipitation around geysers and hot-spring vents, North Island, New Zealand. J. Sediment. Res. 67, 88–104.
Jones, B., Renaut, R.W., Rosen, M.R., 2003. Silicified microbes in a geyser mound: the enigma of low-temperature cyanobacteria in a high-temperature setting. Palaios 18, 87–109.
Jones, B., Renaut, R.W., Rosen, M.R., 2004. Taxonomic fidelity of silicified filamentous microbes from hot spring systems in the Taupo Volcanic Zone, North Island, New Zealand. Trans. R. Soc. Edinb. Earth Sci. 94, 475–483.
Konhauser, K.O., Ferris, F.G., 1996. Diversity of iron and silica precipitation by microbial mats in hydrothermal waters, Iceland: implications for Precambrian iron formations. Geology 24, 323–326.
Konhauser, K.O., Phoenix, V.R., Bottrell, S.H., Adams, D.G., Head, I.M., 2001. Microbial–silica interactions in Icelandic hot spring sinter: possible analogues for some Precambrian siliceous stromatolites. Sedimentology 48, 415–433.
Konhauser, K.O., Jones, B., Reysenbach, A., Renaut, R.W., 2003. Hot spring sinters: keys to understanding Earth's earliest life forms. Can. J. Earth Sci. 40, 1713–1724.
Lahsen, A., Trujillo, P., 1976. El Tatio Geothermal Field. Proceedings of the 2nd United Nations Symposium on Geothermal Fields, Berkeley, California, pp. 157–178.
Landrum, J.T., Bennett, P.C., Engel, A.S., Alsina, M.A., Pastén, P.A., Milliken, K., 2009. Partitioning geochemistry of arsenic and antimony, El Tatio Geyser Field, Chile. Appl. Geochem. 24, 664–676.
Lowe, D.R., Braunstein, D., 2003. Microstructure of high-temperature (>73 C) siliceous sinter deposited around hot springs and geysers Yellowstone National Park: the role of biological and abiological processes in sedimentation. Can. J. Earth Sci. 40, 1611–1642.
Lowe, D.R., Anderson, K.S., Braunstein, D., 2001. The zonation and structuring of siliceous sinter around hot springs, Yellowstone National Park, and the role of thermophilic bacteria in its deposition. In: Reyesenbach, A.-L., Voytek, M., Mancinelli, R. (Eds.), Thermophiles: Biodiversity, Ecology, and Evolution. Kluwer Academic/Plenum Publishers, New York, pp. 143–166.
Lynne, B.Y., 2007. Diagenesis of Siliceous Sinter Deposits in the U.S.A. and New ZealandPh. D. Thesis University of Auckland, New Zealand (189 pp.).
Lynne, B.Y., 2012. Mapping vent to distal-apron hot spring paleo-flow pathways using siliceous sinter architecture. Geothermics 43, 3–24.
Lynne, B.Y., Campbell, K.A., 2003. Diagenetic transformations (opal-A to quartz) of low- and mid-temperature microbial textures in siliceous hot-spring deposits, Taupo Volcanic Zone, New Zealand. Can. J. Earth Sci. 40, 1679–1696.
Lynne, B.Y., Campbell, K.A., 2004. Morphologic and mineralogic transitions from opal-A to opal-CT in low-temperature siliceous sinter diagenesis, Taupo Volcanic Zone, New Zealand. J. Sediment. Res. 74, 561–579.
Lynne, B.Y., Campbell, K.A., Moore, J.N., Browne, P.R.L., 2005. Diagenesis of 1900-year-old siliceous sinter (opal-A to quartz) at Opal Mound, Roosevelt Hot Springs, Utah, U.S.A. Sediment. Geol. 179, 249–278.
Lynne, B.Y., Campbell, K.A., James, B., Browne, P.R.L., Moore, J.N., 2007. Tracking Crystallinity in Siliceous Hot-Spring Deposits. Am. J. Sci. 307, 612–641.
Lynne, B.Y., Campbell, K.A., Moore, J.N., Browne, P.R.L., 2008. Origin and evolution of the Steamboat Springs siliceous sinter deposit, Nevada, U.S.A. Sediment. Geol. 210, 111–131.
Mountain, B.W., Benning, L.G., Boerema, J., 2003. Experimental studies on New Zealand hot spring sinters: Rates of growth and textural development. Can. J. Earth Sci. 40, 1643–1667.
Phoenix, V.R., Adams, D.G., Konhauser, K.O., 2000. Cyanobacterial viability during hydrothermal biomineralisation. Chem. Geol. 169, 329–338.
Pierson, B.K., Castenholz, R.W., 1974. A phototrophic gliding filamentous bacterium of hot springs, Chloroflexus aurantiacus. Arch. Microbiol. 100, 5–24.
Pope, J.G., McConchie, D.M., Clark, M.D., Brown, K.L., 2004. Diurnal variations in the chemistry of geothermal fluids after discharge, Champagne Pool, Waiotapu, New Zealand. Chem. Geol. 203, 253–272.
Rodgers, K.A., Greatrex, R., Hyland, M., Simmons, S.F., Browne, P.R.L., 2002a. A modern, evaporitic occurrence of teruggite, $Ca_4MgB_{12}As_2O_{28} \cdot 18H_2O$, and nobleite, $CaB_6O_{10} \cdot 4H_2O$, from the El Tatio geothermal field, Antofagasta Province, Chile. Mineral. Mag. 66, 253–259.
Rodgers, K.A., Cook, K.L., Browne, P.R.L., Campbell, K.A., 2002b. The mineralogy, texture and significance of silica derived from alteration by steam condensate in three New Zealand geothermal fields. Clay Miner. 37, 299–322.
Rodgers, K.A., Browne, P.R.L., Buddle, T.F., Cook, K.L., Greatrex, R.A., Hampton, W.A., Herdianita, N.R., Holland, G.R., Lynne, B.Y., Martin, R., Newton, Z., Pastars, D., Sannazarro, K.L., Teece, C.I.A., 2004. Silica phases in sinters and residues from geothermal fields of New Zealand. Earth-Sci. Rev. 66, 1–61.
Schinteie, R., Campbell, K.A., Browne, P.R.L., 2007. Microfacies of stromatolitic sinter from acid–sulphate–chloride springs at Parariki stream, Rotokawa Geothermal Field, New Zealand. Palaeontol. Electron. 10, (33 pp.).
Smith, B.Y., Turner, S.J., Rodgers, K.A., 2003. Opal-A and associated microbes from Wairakei, New Zealand: the first 300 days. Mineral. Mag. 67, 563–579.
Tassi, F., Martinez, F., Vaselli, O., Capaccioni, B., Viramonte, J., 2005. Light hydrocarbons as redox and temperature indicators in the geothermal field of El Tatio (northern Chile). Appl. Geochem. 20, 2049–2062.
Tassi, F., Aguilera, F., Darrah, T., Vaselli, O., Capaccioni, B., Poreda, R.J., Delgado Huertas, A., 2010. Fluid geochemistry of hydrothermal systems in the Arica-Parinacota, Tarapacá and Antofagasta regions (northern Chile). J. Volcanol. Geotherm. Res. 192, 1–15.
Tobler, D.J., Stefansson, A., Benning, L.G., 2008. In situ grown silica sinters in Icelandic geothermal areas. Geobiology 6, 481–502.
Walter, M.R., 1976. Hot-springs sediments in Yellowstone National Park. In: Walter, M.R. (Ed.), Stromatolites. Developments in Sedimentology. Elsevier, Amsterdam, pp. 489–498.
Walter, M.R., Des Marais, D., Farmer, J.D., Hinman, N.W., 1996. Lithofacies and biofacies of mid-Paleozoic thermal spring deposits in the Drummond basin, Queensland, Australia. Palaios 11, 497–518.
Walter, M.R., McLoughlin, S., Drinnan, A.N., Farmer, J.D., 1998. Palaeontology of Devonian thermal spring deposits, Drummond basin, Australia. Alcheringa 22, 285–314.
Westall, F., de Wit, M.J., Dann, J., van der Gasst, S., de Ronde, C.E.J., Gerneke, D., 2001. Early Archean fossil bacteria and biofilms in hydrothermally-influenced sediments from the Barberton greenstone belt, South Africa. Precambrian Res. 106, 93–116.
White, D.E., Hutchinson, R.A., Keith, T.E.C., 1988. The geology and remarkable thermal activity of Norris Geyser Basin, Yellowstone National Park, Wyoming. US Geol. Surv. Prof. Pap. 1456 (84 pp.).
Zhou, J., Lau, K.M., 1998. Does a monsoon climate exist over South America? J. Clim. 11, 1020–1040.